Tailoring colors by O-annulation of polycyclic aromatic hydrocarbons

Tanja Miletić,[a,b] Andrea Fermi,[b,c] Ioannis Orfanos,[d,e] Aggelos Avramopoulos,[f] Federica De Leo,[c] Nicola Demitri,[g] Giacomo Bergamini,[h] Paola Ceroni,[h] Manthos G. Papadopoulos,[f] Stelios Couris[d,e] and Davide Bonifazi*[a,b,c]

Abstract: The synthesis of O-doped polyaromatic hydrocarbons, in which two polycyclic aromatic hydrocarbon subunits are bridged through one or two O atoms, has been achieved. This includes high-yielding ring-closure key steps that, depending on the reaction conditions, yield the formation of either furanyl or pyranopyranyl linkages through intramolecular C-O bond formation. Comprehensive photophysical measurements in solution showed that these molecules feature exceptionally high emission yields and tunable absorption properties throughout the UV-vis spectral region. Electrochemical investigations showed that in all cases the O-annulation increases the electron donor capabilities by raising the HOMO energy level with the LUMO energy level being less affected. Moreover, third-order NLO measurements of solutions or thin films containing the dyes displayed very good second hyperpolarizibility values. Importantly, PMMA films containing the pyranopyranyl derivatives displayed weak linear absorption and NLO absorption compared to the nonlinearity and NLO refraction, respectively, revealing to be exceptional organic materials for photonic devices.

Introduction

Amongst the plethora of organic semiconductors available, polycyclic aromatic hydrocarbons (PAHs) have certainly attracted an increasing attention.[1–6] With respect to infinite graphene, PAHs display non-zero tunable bandgaps and are thus of use as chromophores in antennae[7–12] or emissive molecular architectures[13–19] and in general in all optoelectronic applications requiring a tunable semiconducting material.[6,20] Exploiting the organic synthetic tools,[21,22] one can tune the molecular HOMO-LUMO gap[8] either by: *i*) changing the size and edge of the carbon-based aromatic framework; *ii*) varying the molecular planarity upon insertion of bulky substituents or bridging chains; *iii*) changing the aromatic properties of the constituting monomeric units; *iv*) varying the peripheral functionalization through the insertion of electron-donating or -withdrawing substituents; *v*) inclosing structural "defects"; *vi*) promoting supramolecular interactions between individual molecules governing their organization into a condensed phase or *vii*) replacing selected carbon atoms by isostructural and isoelectronic analogues (*i.e.*, doping). In particular, the heteroatom doping approach[23,24] is increasingly becoming important, as significant perturbation of the optoelectronic properties can be obtained without a substantial structural modification.[25–36]

Bottom-up covalent synthesis can be exploited to access structurally defined heteroatom-doped graphene fragments with precise control over the size, periphery, substitution pattern, doping ratio and position.[36,37] In this respect, *peri*-xanthenoxanthene (PXX),[38,39] the O-doped analogue of anthanthrene, can be conceptualized as a building unit for engineering a new class of O-doped PAHs. Substituted PXX derivatives are characterized by excellent carrier transport and injection properties, as well as easy processability, chemical inertness and high-thermal stability.[40,41] Due to these properties, PXX has proven exceptional performance when used as active organic semiconductor (OSC) in transistors for rollable OLEDs.[42,43] In particular, it has been proven that the good performances are triggered by (*i*) the good charge transport properties and (*ii*) the good thermal and chemical stability against parasitic oxidations occurring at the periphery of the π-conjugated system.[41,44]

Capitalizing on these hetero-doped structures, we have reported very recently the synthesis of a series of O-doped isosteres of benzorylenes, in which peripheral carbon atoms are replaced by oxygen atoms at the armchair edges exploiting the *Pummerer*-modified Cu(I)-catalyzed ring-closure reaction, involving intramolecular C-O bond formation as the planarization reaction.[45] Aiming at studying the effect of the π-extension of the carbon framework, here we report on the preparation of π-extended PXX derivatives through the fusion of two PAH subunits (Figure 1). In our approach, we have considered the extended PXX derivatives reflecting bishydroxyPAHs with 2-hydroxyperylene and 2-hydroxynaphthalene moieties as the key constituting units. At

[a] Dr. T. Miletić, Prof. Dr. D. Bonifazi
Department of Chemical and Pharmaceutical Sciences, INSTM UdR Trieste, University of Trieste, Piazzale Europa 1, 34127 Trieste (Italy)
[b] Dr. T. Miletić, Dr. A. Fermi, Prof. Dr. D. Bonifazi
School of Chemistry, Cardiff University
Park Place, CF10 3AT, Cardiff (United Kingdom)
E-mail: bonifazid@cardiff.ac.uk.
[c] Dr. A. Fermi, Dr. F. De Leo, Prof. Dr. D. Bonifazi
Department of Chemistry, University of Namur (UNamur), 61 Rue de Bruxelles, Namur 5000 (Belgium)
[d] G. Orfanos, Prof. Dr. S. Couris
Department of Physics, University of Patras, 26504 Patras (Greece)
[e] G. Orfanos, Prof. Dr. S. Couris
Institute of Chemical Engineering Sciences (ICE-HT), Foundation for Research and Technology-Hellas (FORTH), P.O. Box 1414, Patras 26504 (Greece)
[f] Dr. A. Avramopoulos, Dr. M. G. Papadopoulos
Institute of Biology, Medicinal Chemistry and Biotechnology, National Hellenic Research Foundation, 48 Vas. Constantinou Avenue, Athens 11635 (Greece)
[g] Dr. N. Demitri
Elettra – Sincrotrone Trieste, S.S. 14 Km 163.5 in Area Science Park, 34149 Basovizza – Trieste (Italy)
[h] Dr. G. Bergamini, Prof. Dr. P. Ceroni
Department of Chemistry «Giacomo Ciamician», University of Bologna, Via Selmi 2, 40126 Bologna (Italy)

Supporting information for this article is given via a link at the end of the document.

the synthetic planning level, we contemplated the oxidative Cu(I)-catalyzed planarization reaction developed by us[45] to form the pyranopyranyl motif (Figure 1). Indulging this synthetic protocol, the easily prepared bishydroxyPAHs precursors[46–55] give us the opportunity to alternatively fuse the PAHs through furanyl linkages[56] following an acid-catalyzed cyclization strategy (Figure 1). Photophysical and electrochemical characterizations showed that complementary spectroscopic and redox properties can be tailored through a fine tuning of both the π-extension of the carbon scaffold and the oxygen linkages (*i.e.*, furanyl *vs* pyranopyranyl rings), ultimately covering the visible absorption and emission spectral region. All derivatives display high absorption values and strong emissions. Non-linear optical (NLO) responses of all O-doped polyaromatics were also investigated both in solution and as thin-films by Z-scan technique, employing 35 ps, 532 nm (Vis) laser excitation. All showed strong second hyperpolarizabilities values, as completely predicted by theoretical calculations performed at the CAM-B3LYP/6-31+G** level of theory. To ease the description of the different substitution patterns around the two fundamental furanyl and pyranopyranyl cores, the nomenclature depicted in Figure 1 will be used throughout this manuscript. Being the fundamental cores of the two molecular families composed of either a binaphthofurane or a PXX, each subnaphthyl ring can be differently π-extended. In accordance with this general scheme, a labeling nomenclature is proposed, where the n and m indexes indicate the possible π-extension of the carbon framework expressed as a number of C-C fused naphthyl rings.

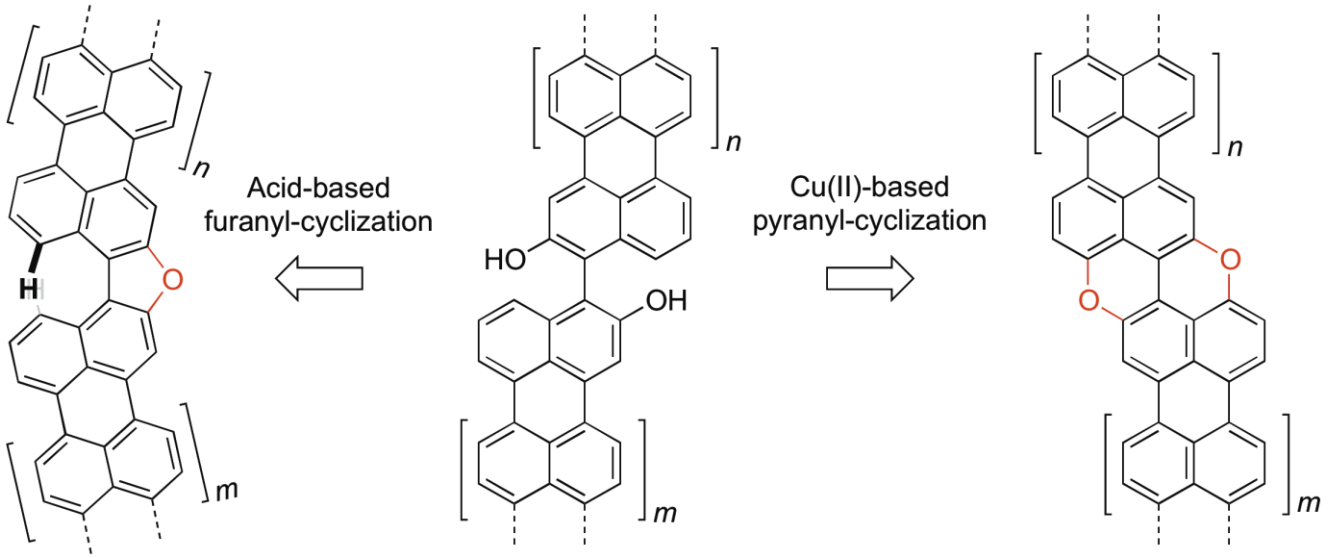

Figure 1. Fusion of PAHs through furanyl (right) and pyranopyranyl (left) cyclization strategies (*n* and *m* indexes indicate the possible π-extension of the carbon framework expressed as a number if C-C fused naphthyl rings).

Results and discussion

Synthesis. The synthesis commenced with the preparation of hydroxyl-perylene 2 (Scheme 1). Friedel-Craft alkylation of perylene, following the protocol by *Pillow et al.*[57] in the presence of a large excess of *t*BuCl,[58–60] leads to an inseparable mixture of di-, tri- and tetra substituted *t*Bu-perylene derivatives. The unpurified perylene mixture was subsequently submitted to selective C-H borylation reaction in the presence of 10 mol% of $[Ir(COD)(OMe)]_2$ catalyst and 20 mol% of dtbpy and B_2pin_2 in *n*-hexane at 80 °C for 24 h,[61] allowing the isolation of tetra-*tert*-butylperylene **1a**, mono- and bis-boronic esters **1b** and **1c** (see X-ray structure Section S6, SI) in 33, 20 and 30% yield, respectively. Oxidation of boronic esters **1b** using H_2O_2 and NaOH in THF at r.t.,[62] yielded perylenol derivative **2** in 80-85%. Following the literature synthetic routes for preparing BINOLs,[46–52,54,55,63] we turned our attention toward the Cu-TMEDA-based oxidative C-C bond formation[64,65] as dimerization reaction. Thus, homodimerization of perylenol **2** was performed in the presence of [Cu(OH)Cl•TMEDA] catalyst under air at 20 °C in CH_2Cl_2, to give bisperylenol **4** in 71% yield. Small transparent crystals of **4** were obtained by vapor diffusion of MeOH into a solution of **4** in CH_2Br_2. The asymmetric unit of the crystals contains one independent molecule, which is H-bonded to two MeOH molecules (Figure 2). The molecular structure depicted in Figure 2a, nicely reveals the non-planar arrangement of the two perylene scaffolds with an interplanar angle of 62.8° with the two hydroxyl groups adopting a *syn* conformation. The crystal packing shows the formation of dimeric species held by H-bonding interactions bridged by solvent (MeOH) molecules. Similarly, perylenol **2** was cross-coupled with 2-naphthol to give naphthalenylperylene derivative **3** in 26% yield (homodimers bisperylenol **4** and BINOL were also formed and thus separated by column chromatography). It should be noted that bishydroxyPAHs **3** and **4** were prepared and used as scalemic mixtures. Following the oxidative protocol recently developed by us,[45] the dihydroxy species were subsequently cyclized into the relevant pyranopyran derivatives. Specifically, Cu-catalyzed oxidative intramolecular etherification of dihydroxy derivatives **3** and **4** (CuI and PivOH in DMSO at 140 °C in the air) afforded pyranopyran derivatives $\mathbf{5^{Pp}}$ and $\mathbf{6^{Pp}}$, in 57% and 84% yield, respectively. The structures of all intermediates and products were unambiguously identified by HR-MALDI through the detection of the peak corresponding to the molecular mass (M) and by ^{1}H- and ^{13}C-NMR, UV-Vis, and IR spectroscopy (see Section S3, SI). In particular, HR-MALDI showed the peak related to the molecular mass (M) at m/z 574.2889 ($C_{42}H_{38}O_2$, calc.: 574.2872) and 866.5059 ($C_{64}H_{66}O_2$, calc.: 866.5063), for extended pyranopyran $\mathbf{5^{Pp}}$ and $\mathbf{6^{Pp}}$,

respectively. Unfortunately, ^{13}C-NMR could not be recorded, as both pyranopyranyl derivatives seem to display limited solubility, likely triggered by their great tendency to undergo strong aggregation.

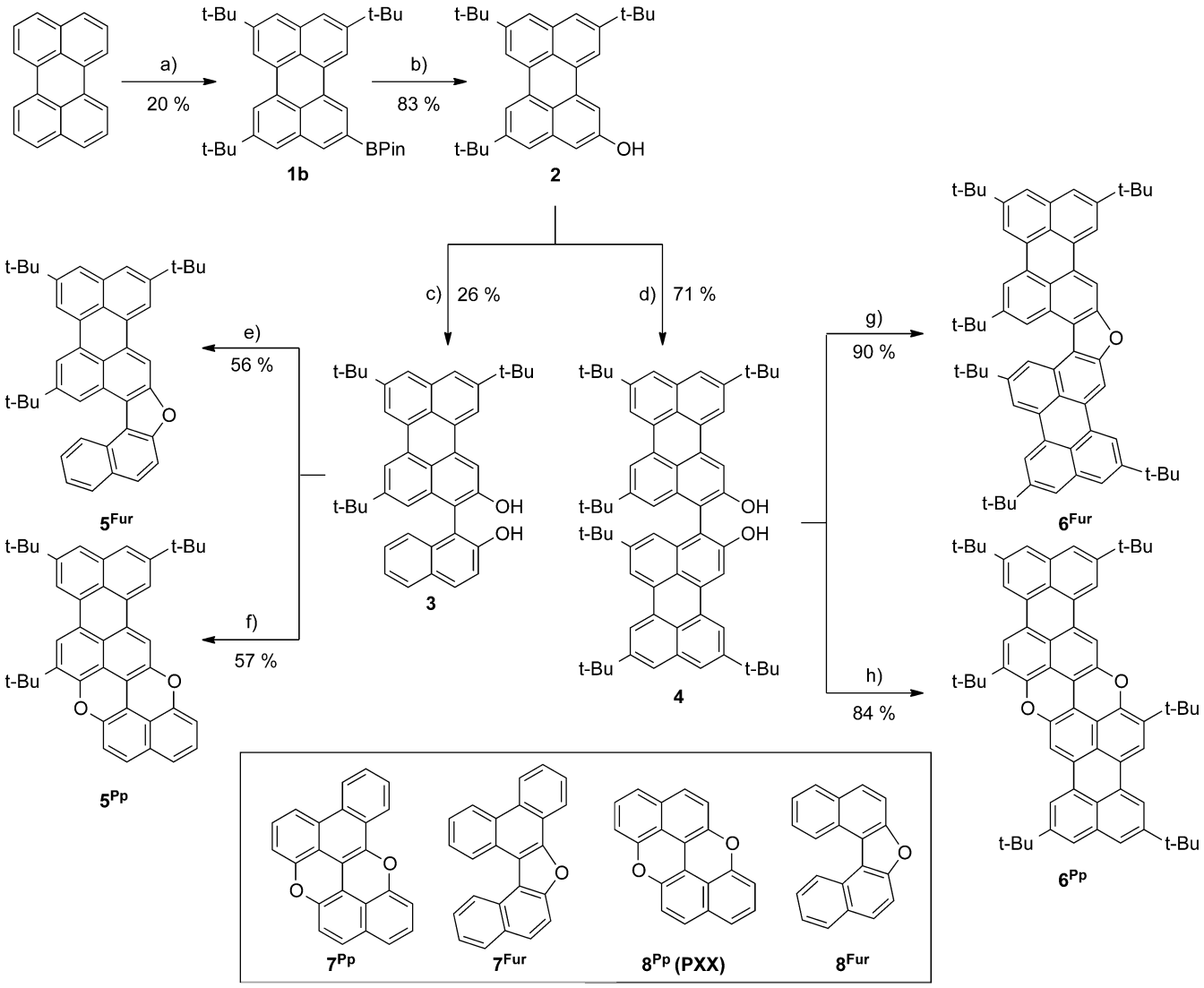

Scheme 1. Synthetic pathway for compounds **1**-**6**$^{Fur/Pp}$. Reagents and conditions: a) 1. $AlCl_3$, *t*-BuCl, ODCB, 0°C to r.t., 24h; 2. $[Ir(COD)(OMe)]_2$, 10 mol%, dtbpy, 20 mol%, B_2Pin_2, *n*-hexane, 80°C, 24h; b) NaOH, H_2O_2 aq. sol. 35 wt%, THF, r.t., 2h; c) 2-naphthol, [Cu(OH)(Cl)TMEDA], air, CH_2Cl_2, 20°C, 2h; d) [Cu(OH)(Cl)TMEDA], air, CH_2Cl_2, 20°C, 1h; e,g) *p*-TsOH, Toluene, reflux, Ar, 4h; f,h) CuI, $(CH_3)_3CCOOH$, DMSO, 140 °C, 2h.

To qualitatively support this assumption, a 2 mM toluene solution of **6**^{Pp} was drop-casted to a silicon wafer. After solvent evaporation, SEM imaging of the remaining powder show the presence of microscale brittle stick-like morphologies (Figure S28, SI). Alternatively, when dihydroxy precursors **3** and **4** were reacted in the presence of *p*-TsOH in a refluxing toluene solution,[66,67] extended furanyl derivatives **5**^{Fur} and **6**^{Fur} could be obtained in 56% and 90% yield. Again, their structures were unambiguously identified by ^{1}H- and ^{13}C-NMR, UV-Vis, and IR spectroscopies, with the HR-MALDI showing the peak corresponding to the molecular mass at m/z 560.3079 ($C_{42}H_{40}O$, calc.: 560.3079) and 852.5268 ($C_{64}H_{68}O$, calc.: 852.5270) for extended furanes **5**^{Fur} and **6**^{Fur}, respectively. Reference compounds **7**$^{Fur/Pp}$ and **8**$^{Fur/Pp}$ (Scheme 1) were also prepared following similar synthetic strategies to those developed for compounds **5** and **6** (Scheme S1, SI). To further corroborate the chemical structure of the cyclized derivatives, crystals suitable for X-ray diffraction analysis were obtained either by vapor diffusion or slow solvent evaporation of solutions containing the relevant product (Figures 3-5, for the detailed crystallization procedures refer to SI). Despite the many attempts, no suitable crystals were obtained for the pyranopyran derivatives, and only those obtained for the furanyl derivatives will be discussed in this paper.

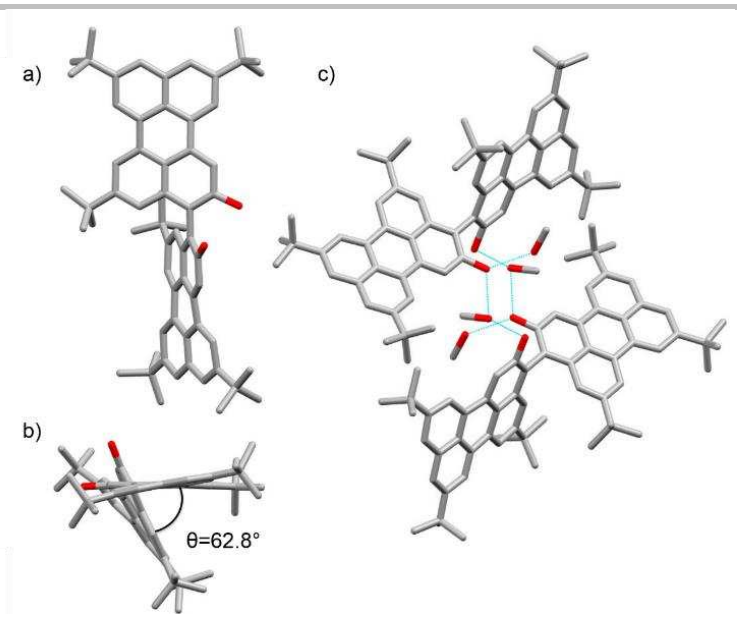

Figure 2. a) Top-view and b,c) side-views of the crystal structure and packing of bisperynol derivative **4** (space group: *P*-1; atom colors: red O, grey C; hydrogens omitted for clarity). Notably, the hydroxyl groups of the bisperynols are engaged in H-bonding interactions through two bridging MeOH solvent molecules forming dimeric species at the solid state.

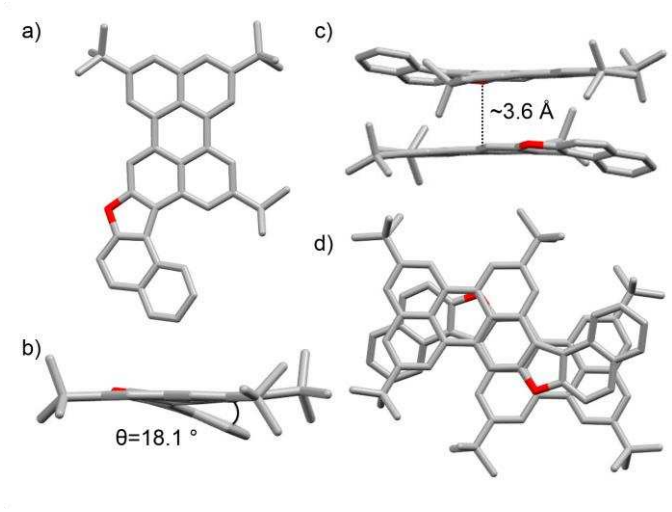

Figure 3. a,d) Top-views and b,c) side-views of the crystal structure and π-π packing arrangement of furanyl derivative **5^{Fur}** (center, space group: *P* 2_1/c; atom colors: red O and grey C; hydrogens omitted for clarity). Crystals obtained from slow vapor diffusion of MeOH to a C_6D_6 solution.

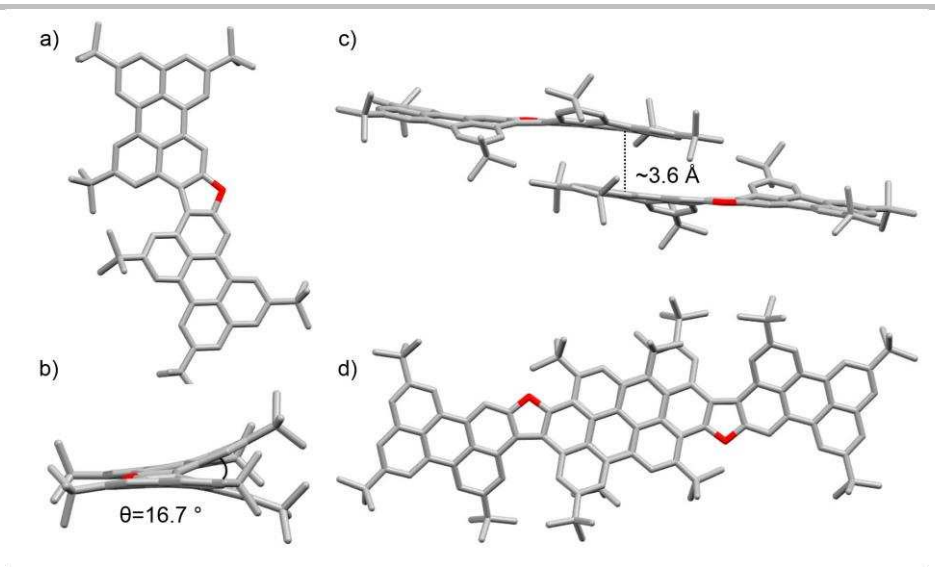

Figure 4. a,d) Top-views and b,c) side-views of the crystal structure and π-π stacking arrangement of furanyl derivative **6**^{Fur} (bottom, space group: *P* 2/c; atom colors: red O and grey C; hydrogens omitted for clarity). Crystals obtained from slow evaporation of a C_6D_6/hexane solution.

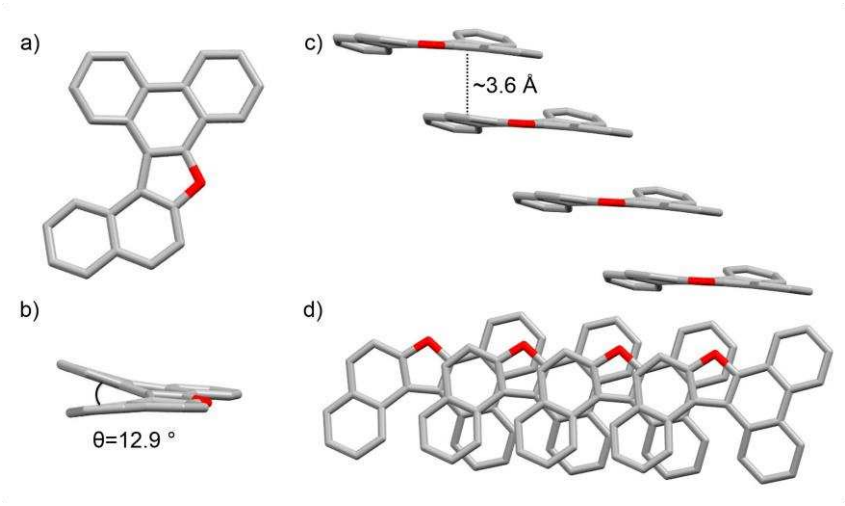

Figure 5. a,d) Top-views and b,c) side-views of the crystal structure and π-π packing arrangement of furanyl derivative **7**^{Fur} (space group: *P* $2_12_12_1$; atom colors: red O and grey C; hydrogens omitted for clarity). Crystals obtained from slow evaporation of a CH_2Cl_2 solution.

All the X-ray structures of **5**^{Fur}-**7**^{Fur} confirm the presence of the furanyl ring. Looking at their organization at the solid state (Figures 3-5c,d), one can clearly evidence the presence of columnar arrangements in which the molecules are organized in π-π stacks, with a similar average interplanar spacing of ~3.6 Å for derivatives **5**^{Fur}, **6**^{Fur} and **7**^{Fur}. As expected, the presence of the five-membered cycle induces a significant distortion of the PAH moieties due to C-H···H-C repulsive interactions (see also Figure 1), triggering interplanar angles of ~18.1, ~16.7 and ~12.9° for **5**^{Fur}, **6**^{Fur} and **7**^{Fur}, respectively. Notably, the presence of the highly hindering *t*Bu groups in molecules **5**^{Fur} and **6**^{Fur} further raises the interplanar angle. While furane **5**^{Fur} antiparallely stacks into a columnar arrangement with no lateral off-set, molecules **6**^{Fur} and **7**^{Fur} form off-set solid-state organizations. In particular, bisperylene furane **6**^{Fur} organizes through perylene-perylene stacks with a lateral off-set of 3.5(1) Å, whereas phenanthrenenaphtyl furane **7**^{Fur} undergoes off-set π-π stacking involving the naphthalene and phenanthrene moieties. The thermal stability of compounds **4**, **6**^{Fur}, **6**^{Pp} were investigated by thermogravimetric analysis (TGA) and compared with reference compound **8**^{Pp}. While molecule **8**^{Pp} starts to sublimate at 188°C reaching its maximum at 265°C (see also DTG profile, Figure S35a, SI), the TGA profiles of compounds **4**, **6**^{Fur} and **6**^{Pp} showed very high thermal stability under N_2, with sublimation temperatures centered at 320, 340 and 400°C, respectively (Figures S35b-d, SI). The thermal stability of extended pyranopyran derivative **6**^{Pp} was also evaluated in the air with a scan rate of 10°C min^{-1}. The TGA profile (Figure S36, SI) only displays a significant weight loss above 370°C, suggesting that molecule **6**^{Pp} can stand the critical environmental conditions typical of a fully-operative device, namely under O_2 and high temperatures.

Absorption and emission spectroscopic investigations. The effects of increasing the conjugation for both furanyl and pyranopyranyl derivatives have been evaluated by steady-state UV-Vis absorption and emission spectroscopies, and the key data are gathered in Table 1. In general, all compounds show high molar absorption coefficients (up to 10^5 $M^{-1}cm^{-1}$) spanning from the blue to the red region of the visible spectrum, with luminescence lifetimes consistent with singlet radiative deactivations (τ=2–6 ns). Quantum yields are remarkably high across the visible spectrum, with the pyranopyranyl derivatives showing lower emission quantum efficiencies (average Φ value of ~0.5) with respect to the homologous furanyl molecules (average Φ value of ~0.8).

Table 1. Optical properties for compounds O-doped PAHs in toluene solutions.

Molecule	λ (nm)[a], ε (M^{-1} cm^{-1})	λ_{em} (nm)[b]	Φ	τ (ns)
7^{Fur}	352, 26900	371	0.43	5.7
7^{Pp}	446, 14100	452	0.48	4.8
2	445, 25600	463	0.55	4.9
3	452, 33700	508	0.66	3.7
4	463, 65 000	472	0.88	2.7
5^{Fur}	477, 47300	494	0.84	3.0
5^{Pp}	556, 36300	569	0.50	3.8
6^{Fur}	534, 97 400	547	0.80	3.0
6^{Pp}	639, 66400	649	0.52	2.2

[a]UV-vis absorption maximum of the lowest energy band in toluene. [b]Emission maximum in toluene at 25 °C.

Taking into account singly-bonded naphthol-perylenol **3** and conjugated derivatives **5^{Fur}** and **5^{Pp}**, clear bathochromic shifts both in the absorption and in the emission spectra are evidenced when passing from the non-planar to the planarized derivatives (Figure 6a), with the relevant pyranopyranyl molecule displaying the larger red shifts if compared to the furanyl analogue. An equivalent trend is also observed with perylenol **2**, its singly-linked dimer **4** and molecules **6^{Fur}** and **6^{Pp}**, showing largely tunable absorption and emission energies that fall in the red spectral region for the O-annulated derivatives (Figure 6b). Comparing these results with those reported in the literature with all-carbon PAHs displaying comparable visible absorption energies,[68-71] our steady-state studies suggest that, although providing significant bathochromic shifts, the C-O planarization does not dramatically suppress the emission quantum yields as opposed to the formation of the C-C bonds in planar rylenes, the latters usually displaying strong absorptivities but faint luminescence outputs.[72,73]

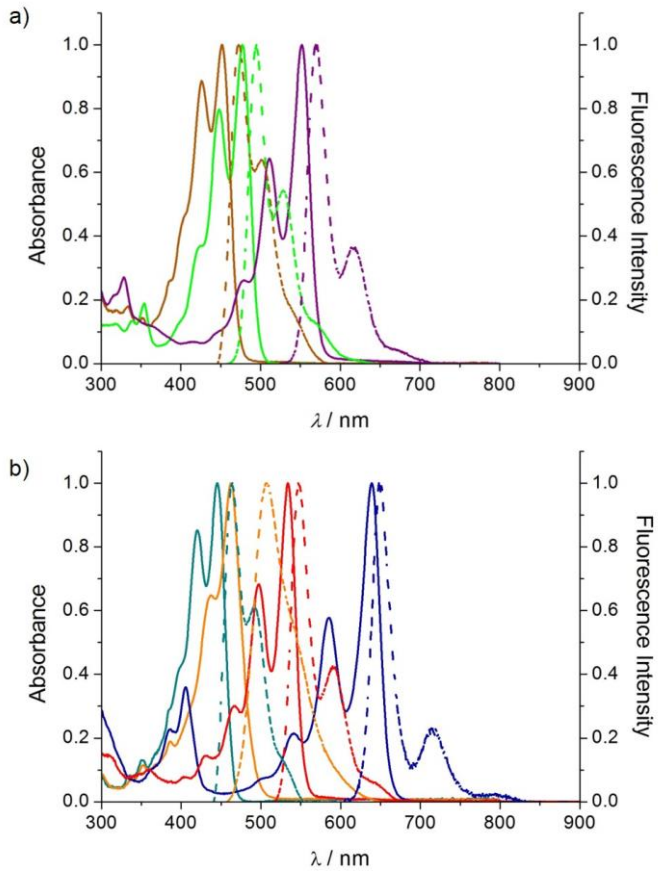

Figure 6. a) Normalized absorption (—) and emission (·····) spectra in toluene at 25°C of a) naphthol-perylenol series: **3** (dark yellow), **5^{Fur}** (green) and **5^{Pp}** (purple) and b) bis-perylenol series: **2** (cyan), **4** (orange), **6^{Fur}** (red) and **6^{Pp}** (blue).

To probe the solid-state emissive properties of all conjugates,[56] different molding solvents[74] were screened to reproducibly obtain solid morphologies of defined shape. Furanes **5^{Fur}** and **6^{Fur}** and pyranopyrans **5^{Pp}** and **6^{Pp}** were initially investigated. Among the different conditions, we found that the slow addition of MeOH to a THF solution of the relevant dye gives rise to a colloidal cloudy solution that, upon prolonged times, undergoes precipitation leading to crystalline powdery solids. SEM imaging analysis (Figure 7) of the dried powder, shows the formation of well-defined and reproducible structures at the microscale featuring different morphologies depending on the chemical structure of the crystallizing molecule. Specifically, compound **5^{Fur}** leads to the formation of elongated hexagonal prisms (Figures 7a-b), 1 µm large and wide, with a length in the order of 5-10 µm. It is noteworthy to underline that needle-like structures, longer than the average prisms, were also present in the sample. On the other side, molecule **5^{Pp}** forms 3-10 µm long stick-like morphologies, featuring thinner diameters (Figures 7c-d). Passing to the bisperyleno derivatives, compound **6^{Fur}** arranges in disk-like structures with a diameter in the micrometer range (Figures 7e-f), while **6^{Pp}** forms rod-like shapes (Figures 7g-h) also featuring microscopic dimensions (for more images see also Figure S29, SI).

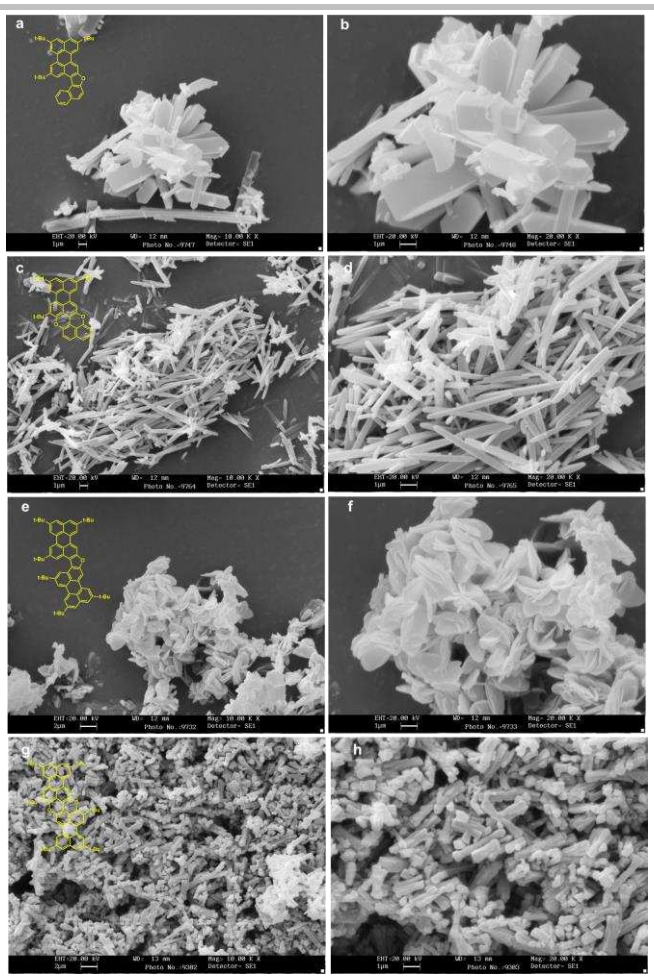

Figure 7. SEM images of the organic nanostructures obtained from a THF solution upon addition of MeOH for molecules **5**^{Fur} (a, b), **5**^{Pp} (c, d), **6**^{Fur} (e, f) and **6**^{Pp} (g, h).

The recorded solid-state emission spectra for compounds **5**^{Fur}, **6**^{Fur} and **7**^{Fur} are depicted in Figure 8. Both model compounds **8**^{Fur} and **8**^{Pp} show appreciable luminescence upon excitation of the powders at room temperature: while **8**^{Fur} displays a blue emission with a structured spectrum featuring maximum at around 400 nm, its pyranopyranyl derivative **8**^{Pp} appears as a yellow-green emitter with a broad spectrum with a maximum at around 545 nm (Figure S44, SI). Owing to the narrowing effect of the pyrano conjugation, also the solid-state emission spectrum of pyrano **8**^{Pp} displays a marked red-shifted profile if compared to that of **8**^{Fur}. The extension of the π-surface of molecule **8**^{Pp} negatively affects the solid-state emissive properties, namely the luminescence outputs of solids obtained from molecules **5**^{Pp} and **6**^{Pp} are hardly detectable; differently, the increase of the conjugation length of furanyl compounds **5**^{Fur} and **6**^{Fur} does not dramatically affect the solid-state luminescence. Specifically, molecule **5**^{Fur} intensely emits a yellow-orange color, showing a structured emission spectrum with a maximum around 560 nm, whereas **6**^{Fur} strongly luminesces, displaying a vibrational structure and a sharp peak at 645 nm. Although the emission spectra of the amorphous powders of **5**^{Fur}, **6**^{Fur} and **7**^{Fur} resulted in some extent sensitive to prolonged UV excitation, and we cannot therefore determine precisely the value of each luminescence quantum yield, these solid-state emission findings are in agreement with literature data reporting high quantum yield for the naphthofuran derivatives.[56,67] Differences in the emissive properties between the naphthofurans and pyranopyranyl-derivatives at the solid are probably correlated with the structural properties of the respective crystal lattices (see above). For instance, considering that molecule **8**^{Pp} (PXX) is self-organized at the solid-state through π-π stacks,[44] we can hypothesize that all pyranopyranyl derivatives likely undergo similar face-to-face arrangements, the latter organizations most favoring non-radiative decays of the emissive excited states.[15,75,76]

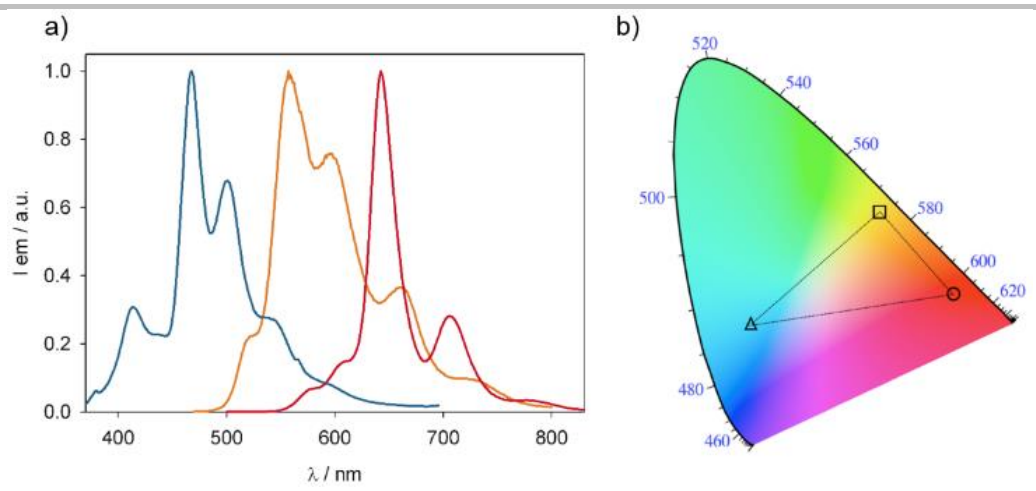

Figure 8. a) emission spectra of **7**^{Fur} (blue line), **5**^{Fur} (orange line), and **6**^{Fur} (red line) in solid samples at r.t. Excitation wavelengths: 360 nm. b) calculated CIE diagram for solid state emissions of **7**^{Fur} (triangle), **5**^{Fur} (square) and **6**^{Fur} (circle). Dotted lines are plotted to display the color gamut accessible by combinations of the three solid emitters.

Electrochemical Investigations. Cyclic voltammetry (CV) in 1,2-dichlorobenzene (ODCB) was used to get further information about the redox properties of compounds **5**$^{Fur/Pp}$-**8**$^{Fur/Pp}$. Their redox potentials *vs.* Fc/Fc^{+} are summarized in Table 2.

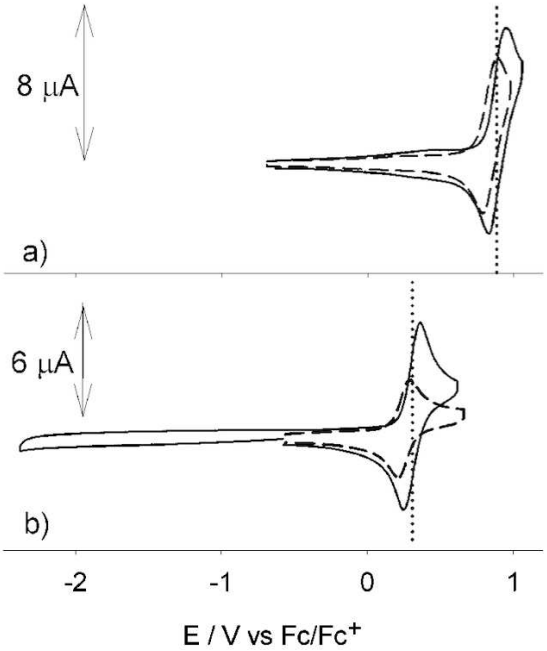

Figure 9. Cyclic voltammetry of a) **8**^{Fur} (0.80 mM, solid line) and **7**^{Fur} (0.75 mM, dashed line); b) **8**^{Pp} (PXX) (0.81 mM, solid line) and **7**^{Pp} (0.43 mM, dashed line). Half-wave oxidation potentials of **8**^{Fur} and **8**^{Pp} (PXX) are evidenced by vertical dotted lines in plots a) and b) respectively, for comparison purposes. Scan rate: 50 mV/s. Supporting electrolyte: $TBAPF_6$. Ferrocene is used as internal reference standard.

Table 2. Half-wave potentials calculated *vs.* the Fc/Fc^{+} couple.

Molecule	$E_{1/2}^{ox1}$ (V)	$E_{1/2}^{ox2}$(V)	$E_{1/2}^{red1}$(V)	$E_{1/2}^{red2}$ (V)
8^{Fur}	0.89 (117)	*nd*	*nd*	*nd*
8^{Pp} (PXX)	0.30 (111)	*nd*	*nd*	*nd*

7^{Fur}	0.84 (100)	*nd*	*nd*	*nd*
7^{Pp}	0.25 (81)	*nd*	*nd*	*nd*
4b	0.30 (133)	0.52 (128)	*-2.37*[a] *(irr)*	*-2.50*[a] *(irr)*
5^{Fur}	0.37 (128)	0.90 (140)	-2.20 (90)	*nd*
5^{Pp}	0.00 (133)	0.56 (122)	-2.25 (101)	*nd*
6^{Fur}	0.20 (127)	0.57 (127)	-2.15 (112)	-2.32 (123)
6^{Pp}	-0.15 (100)	0.32 (107)	-2.16 (100)	-2.26 (120)

Half-wave potentials are calculated as $E_{1/2}=(E_{pa}+E_{pc})/2$ considering anodic (E_{pa}) and cathodic (E_{pc}) peak potentials, unless differently specified. Values in parenthesis are referred to the peak separation (E_{pa}-E_{pc}, in mV) of each reversible process; "*nd*" stands for "not detected" and "*irr*" for an "irreversible process". [a]Determined considering the cathodic peak of an irreversible reduction process.

As depicted in Figures 9a-b, reference molecules **7^{Fur}**-**8^{Fur}** and **7^{Pp}**-**8^{Pp}** each show only a 1-e$^-$, reversible redox couple at similar positive potentials for the furanyl (0.89 and 0.84 V for **8^{Fur}** and **7^{Fur}**) and pyranopyranyl derivatives (0.30 and 0.25 V for **8^{Pp}** and **7^{Pp}**), suggesting that the addition of an extra benzo[a]ring in the molecular structure marginally affects the oxidation potential of the fundamental O-annulated bisnaphthyl derivatives. Notably, no reductions were observed in the electrochemical window of investigation in ODCB. Interestingly, direct comparison of voltammetric behaviors of compounds **8^{Fur}** and **8^{Pp}** evidences the strong electron-donor character of the pyranopyranyl moiety compared to that of furanyl ring, with a significant lowering of the $E_{1/2}{}^{ox1}$ value of ~0.60 V. Concerning the naphthofurane family, the expansion of carbon-based π-surface as in molecules **5^{Fur}** (m = 0, n = 1) and **6^{Fur}** (m = 1, n = 1) dramatically affects the voltammetric behavior compared to that of the reference molecules (Figure 10a-b). Specifically, two monoelectronic and reversible oxidation peaks for **5^{Fur}** appear at 0.37 and 0.90 V as a consequence of the Coulombic interactions between the first and second oxidation holes. Curiously, a first 1-e$^-$ reduction wave also appears as a separated, reversible couple at -2.20 V. As expected, with respect to molecule **8^{Fur}**, the lateral extension of the π-surface through the introduction of a naphthyl unit (m = 0, n = 1) makes molecule **5^{Fur}** a stronger electron-donor. The trend is further evidenced with molecule **6^{Fur}**, featuring symmetrical substitution with two perylenyl units (m = n = 1), which displays even lower oxidation potentials (at 0.20 and 0.57 V for the first and the second wave, respectively); at the same time, two reversible reductions are recorded at similar potentials as those observed for reducing molecule **5^{Fur}**.

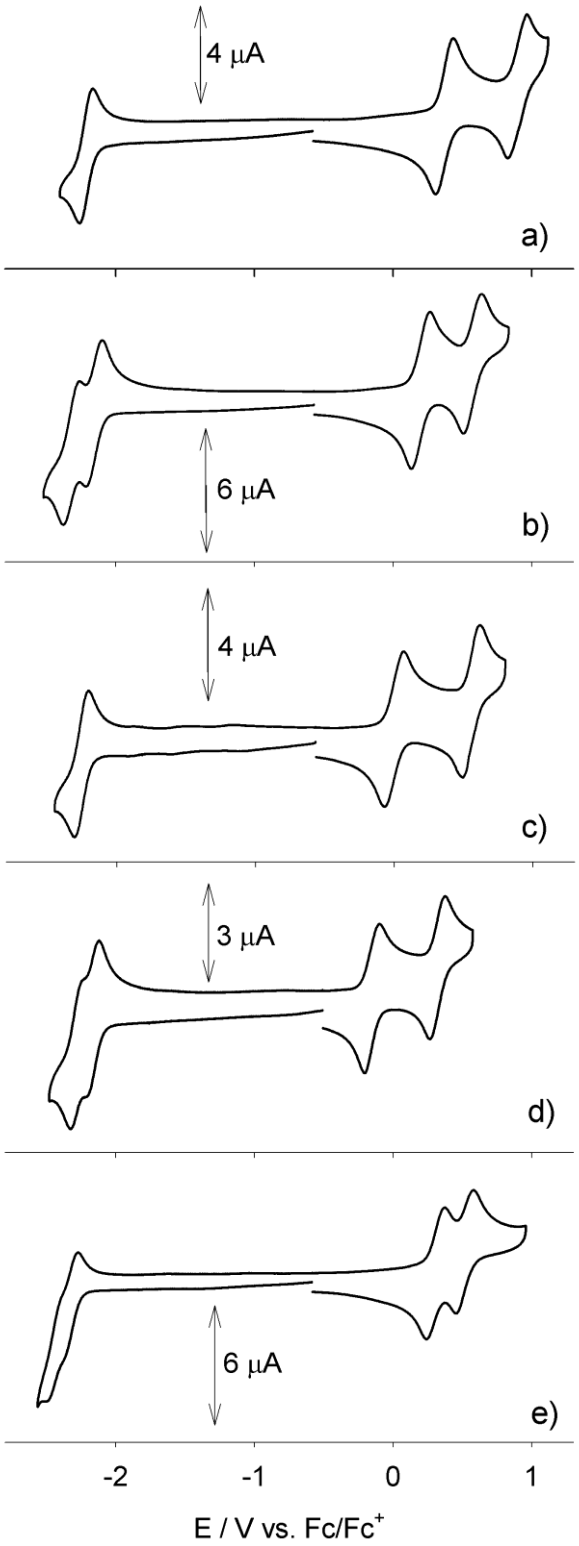

Figure 10. Cyclic voltammetry of molecules a) **5**^{Fur} 0.64 mM, b) **6**^{Fur} 0.63 mM, c) **5**^{Pp} 0.61 mM, d) **6**^{Pp} 0.63 mM, e) **4b** 0.53 mM. Scan rate: 50 mV/s. Supporting electrolyte: $TBAPF_6$. Ferrocene is used as internal reference standard.

As expected, in the case of the PXX-derivatives, the trend is very similar to that described for the naphthofurans family: molecule **5**^{Pp} (m=0, n = 1) features lower oxidation potentials (at *ca.* 0 V vs Fc/Fc^+) if compared to model compound **8**^{Pp}, while a monoelectronic reduction process appears at -2.25 V (Figure 10c). The symmetrical substitution on both sides of the PXX core by two perylenyl units (m = n = 1) makes molecule **6**^{Pp} electron-richer and easier to oxidize than **8**^{Pp}, shifting the first oxidation potential at -0.15 V (Figure 10d). To gain insight on the electronic role of oxygen atoms in the conjugated

system of the PXX-based derivatives, cyclic voltammetry of dimethoxy-biperylene **4b** (see Section S2, SI) was also performed (Figure 10e). Two reversible oxidation processes are detected at 0.30 and 0.52 V, reflecting the weaker electron-donating nature of this structure when compared to that featuring the two oxygen atoms in the π-conjugated pyranopyranyl motif, as in the case of $\mathbf{6^{Pp}}$. Furthermore, we can evidence that the inclusion of the two oxygen atoms in the aromatic system affects significantly the HOMO-LUMO energy gap values (E_g^{CV}, Table 3), which has been experimentally estimated to be 2.67 and 2.01 eV for **4b** and $\mathbf{6^{Pp}}$, respectively.

Table 3. Estimated HOMO-LUMO Energy gap (E_g) for compounds $\mathbf{5^{Fur/Pp}}$-$\mathbf{8^{Fur/Pp}}$ as determined from the optical (E_{00})[a], electrochemical (E_g^{CV}) and theoretical (E_g^{T})[b] studies.

Molecule	E_{00} (nm, eV)	E_g^{CV} (eV)	E_g^{T} (eV)	E_g^{T} (eV)	E_g^{CV} (eV)	E_{00} (nm, eV)	Molecule
$\mathbf{8^{Fur}}$	361, 3.43	---	3.95	3.32	---	449, 2.76	$\mathbf{8^{Pp}}$
$\mathbf{7^{Fur}}$	371, 3.34	---	---	---	---	452, 2.74	$\mathbf{7^{Pp}}$
$\mathbf{5^{Fur}}$	494, 2.51	2.57	2.83	2.50	2.25	569, 2.18	$\mathbf{5^{Pp}}$
$\mathbf{6^{Fur}}$	547, 2.27	2.35	2.48	2.20	2.01	649, 1.91	$\mathbf{6^{Pp}}$

[a]Calculated from the wavelength of the emission maximum in toluene. [b]Calculated bandgap value at the B3LYP/6-31G** gas phase optimized geometry.

From these data it becomes apparent that while the lateral π-extension of the PAHs substructures with a naphthyl unit accounts for a decrease of the E_g^{CV} value of approximately 0.30 V - *cf* the furanyl (left) and pyranopyranyl (right) families in Table 3. Similarly, the O-cyclization of the bishydroxyPAHs strongly affect the E_g^{CV} value, systematically shrinking the gap of *ca*. 0.30 and 0.6 V for the furanyl and pyranopyrayl cycles, respectively (*cf* the furanyl and pyranopyranyl analogues, Table 3 and Figure 11). Notably, an excellent accord between the electrochemical E_g^{CV} and optical E_g values is clearly observable, with the latter being calculated from the λ_{max} of lowest-energy electronic transition. The rainbow collection in Figure 11 perfectly illustrates how the HOMO–LUMO gaps decrease mainly because of the increase of the HOMO energy levels as a consequence of the progressive π-extension and the inclusion of donating furanyl and pyranopyranyl cores. By playing with the type of the O-ring and the number of fused naphthyl rings one can cover the primary colors, moving from yellow furanyl $\mathbf{5^{Fur}}$, to orange bisperylenylfurane $\mathbf{6^{Fur}}$ to pink $\mathbf{5^{Pp}}$ and blue $\mathbf{6^{Pp}}$ pyranopyranyl derivatives. Compared to the tunable core-substituted naphthalenediimides (cNDIs),[77-78] whose color tailoring is achieved through a combination of electron donating substituents in the core leading to push–pull chromophores with the electron withdrawing imide groups,[79] the O-doped PAHs investigated in this work can be considered as valid alternatives for applications in which electronically rich (*i.e.*, high HOMO energy levels) and strongly emissive chromophores are required.[80-82]

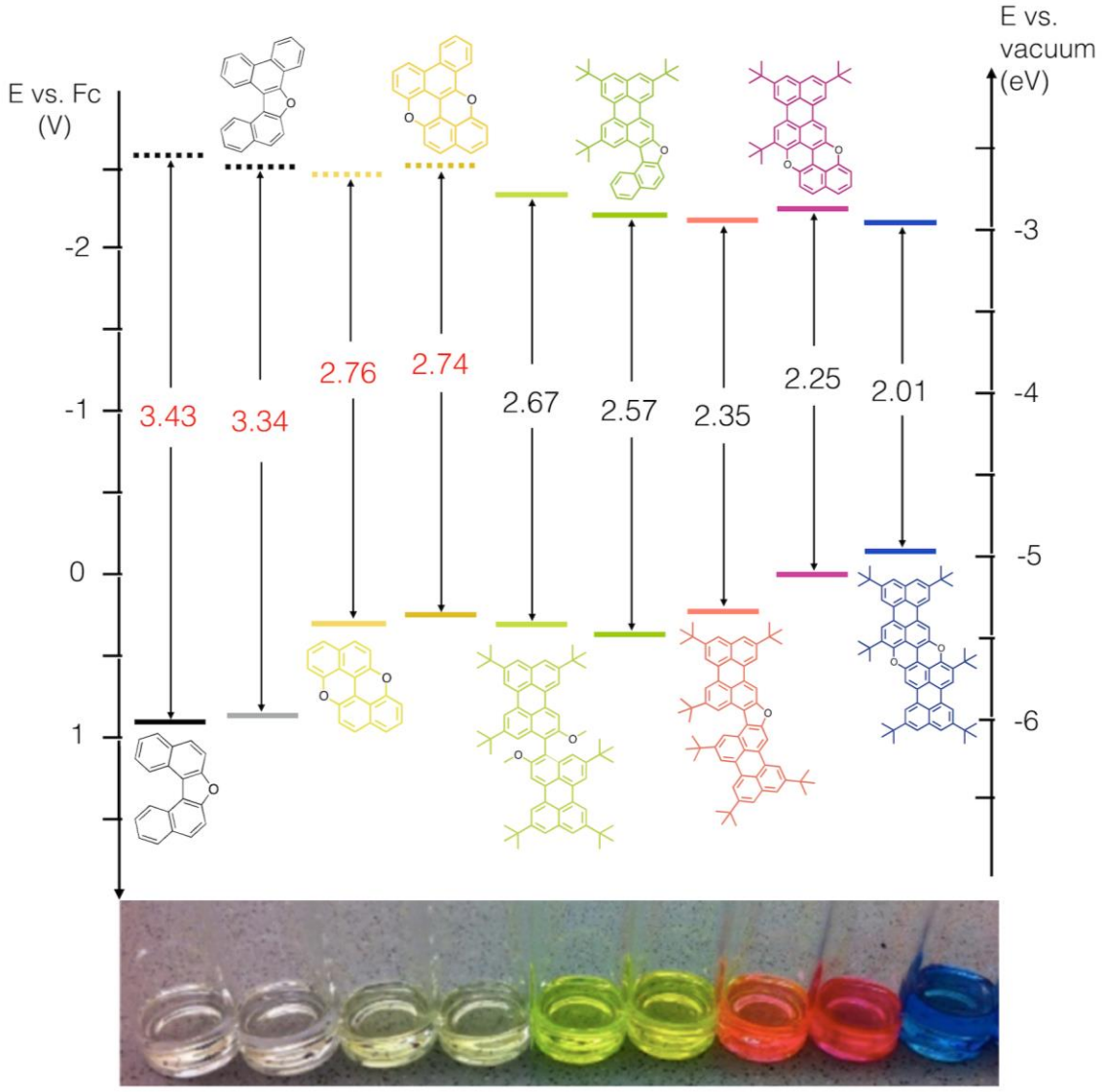

Figure 11. Frontier orbital energies for compounds analyzed by cyclic voltammetry in 1,2-dichlorobenzene (dashed lines corresponding to calculated energies using the optical E_{00}, in red). The formal potential of the Fc/Fc^+ redox couple, taken as a reference, is assumed to be -5.1 eV *vs.* vacuum.

Theoretical modeling. To shed further light on the electronic structure and optical properties of the O-annulated derivatives, the electronic properties of the HOMO and LUMO levels were calculated performing Density Functional Theory (DFT) calculations using the Gaussian 09 package.[83] The results are summarized in Tables 3 and 4. As the *t*Bu substituents have a small effect on the E_{HOMO} and E_{LUMO} energy levels, some of the calculations were performed without the alkyl substituents. Each molecule was modeled in its neutral state performing a geometry optimization and a single point calculation using the Restricted Becke's three-parameter exchange functional,[85] the Lee–Yang–Parr correlation functional[84] (B3LYP/6-31G** level of theory). The crystal structures, when available, were considered as the starting geometries. The HOMO and LUMO orbitals were plotted using the Avogadro software.[86] Other orbitals up to HOMO-4 and LUMO+4 were also calculated (Figures S49-56, SI). It transpires that the molecular HOMO and LUMO orbitals are located on the entire π–surface of the molecules, with the oxygen atoms contributing to the given orbitals differently, depending on the nature of the cyclic linkage. In particular, for the furanyl derivatives the O atom does not significantly contribute to the HOMO orbital, whereas a significant involvement of the O atoms to the HOMO of the pyranopyranyl derivatives is clearly observable (Figure 12). On the contrary, a non-negligible contribution of the O atoms to the LUMO orbitals is noticeable for both O-annulated derivatives. As observed with the electrochemical characterization, the O-cyclization greatly affects the HOMO energy levels (E_{HOMO}), with the pyranopyranyl ring inducing the greatest enhancement of the E_{HOMO} values and thus impacting the most both optical and electrochemical E_g values. On the other hand, the π-extension of the all-carbon aromatic units (m = 0, n = 1 and m = n = 1) affects both E_{HOMO} and E_{LUMO} energy levels, ultimately triggering the decrease of the E_g value as typically observed for π-extended PAHs.[87-89] Notably, the solvent effect (toluene) on the wavelength (λ) for the first allowed electronic transition was also considered in the simulation (Table 4).

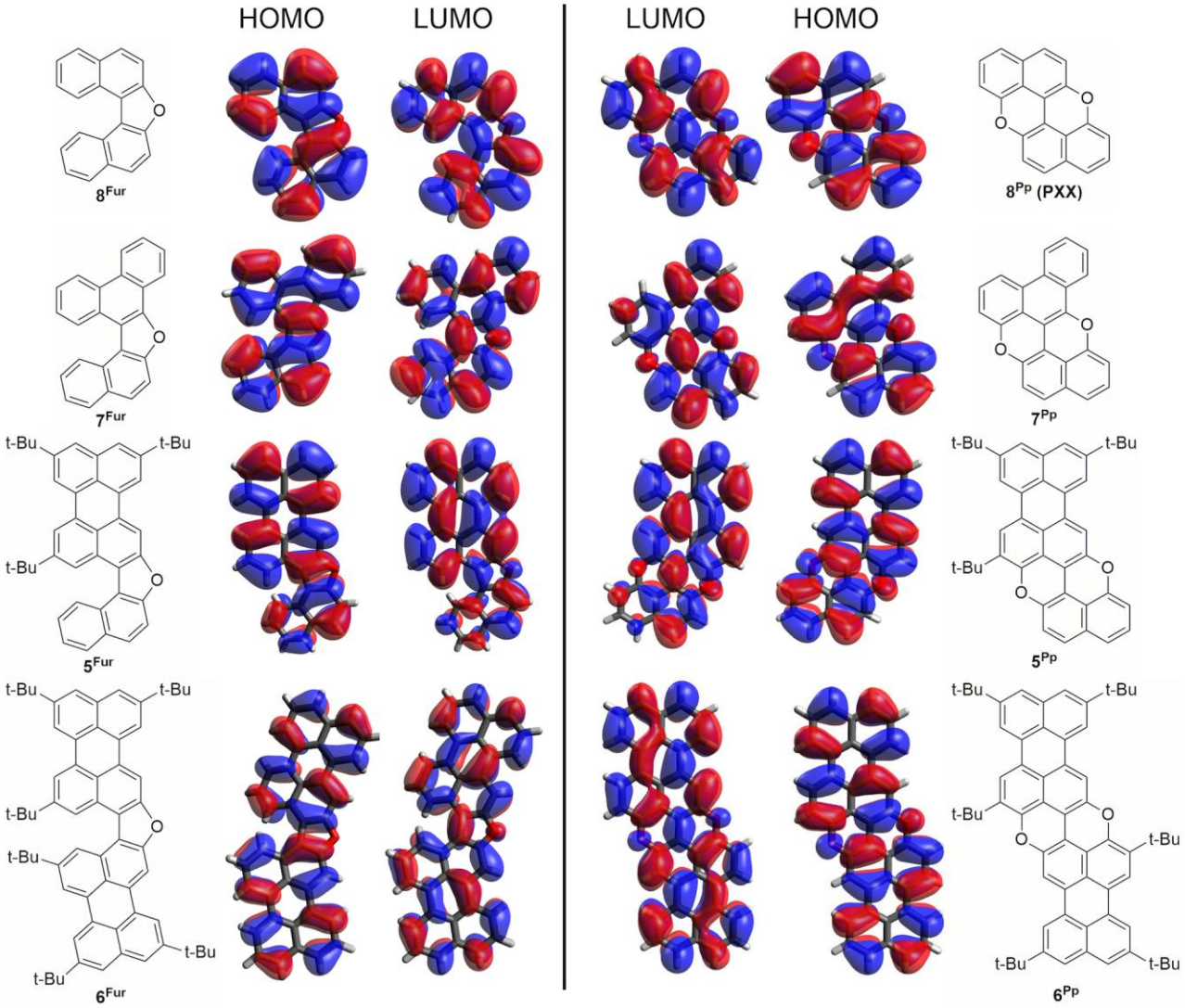

Figure 12. Molecular orbitals for the furanyl (left) and pyranopyranyl (right) derivatives calculated at the B3LYP/6-31G** level of theory.

For both furanyl and pyranopyranyl derivatives, λ increases with n, with the absorption of the pyranopyranyl derivatives being more red-shifted with respect to the furanyl analogues ($\lambda^{Pp} > \lambda^{Fur}$). For **8^{Pp}** a maximum is observed at 400 nm, which lies closely to the absorption (λ = 394.90 nm), whereas the maximum value of **8^{Fur}** is located at λ about 330 nm, which is close to the absorption (λ = 323.09 nm). In Figure S65, the first allowed electronic transitions computed with the aid of natural transition orbital pairs[90] for compounds **8^{Fur}**, **8^{Pp}**, **5^{Fur}**, **5^{Pp}**, **6^{Fur}** and **6^{Pp}** are presented. As one can notice, all electronic transitions occur through π→π* excitations, with the lowest energy absorption band assigned to the HOMO→LUMO transition (see SI for the simulated UV-vis spectra along with the computed bands of the allowed electronic transitions for derivatives **8^{Fur}** and **8^{Pp}**).

Table 4 Computed E_{HOMO},[a] E_{LUMO},[b] E_{HOMO}-E_{LUMO} (E_g^T), absorption wavelength λ (nm), and the excitation energy E_{exc} (eV) for the first allowed electronic transitions. The values were calculated with the CAM-B3LYP/6-31+G**method with explicit solvation (toluene).

Molecule	E_{HOMO} & E_{LUMO} (eV)	E_g^T (eV)	λ (nm)	E_{exc} (eV)	Type of excitation
8^{Fur}	-5.36 & -1.42	3.95	323.09	3.84	HOMO → LUMO (92%)

5^{Fur}	-4.87 & -2.07 -4.73[b] & -1.90[b]	2.80 2.83	446.22 444.87[b]	2.78 2.79	HOMO → LUMO (96.9%)
6^{Fur}	-4.71 & -2.23 -4.54[b] & -2.07[b]	2.48 2.48	496.40 494.02[b]	2.50 2.51[a]	HOMO → LUMO (90.3%)
8^{Pp}	-4.71 & -1.39	3.32	394.9	3.14	HOMO → LUMO (95%)
5^{Pp}	-4.49 & -2.01 -4.38[b] & -1.88[b]	2.48 2.50	502.67 499.96[b]	2.47 2.48[a]	HOMO → LUMO (95.8%)
6^{Pp}	-4.38 & -2.20 -4.25[b] & -2.04[b]	2.18 2.20[b]	565.23 566.72[b]	2.19 2.19[a]	HOMO → LUMO (93.0%)
4	-4.71[b] & -1.96[b]	2.75[b]	438.05[b]	2.83	HOMO→LUMO (50%) HOMO→LUMO+1 (20%)

[a] B3LYP/6-31G**; [b] with *t*Bu group.

Nonlinear Optical (NLO) studies. With these findings in hand, the nonlinear optics (NLO) properties of molecules **4** and **5**$^{Fur/Pp}$, **6**$^{Fur/Pp}$ and **8**$^{Fur/Pp}$ have been systematically investigated using the Z-scan technique, employing visible (532 nm), 35 ps laser pulses from a mode locked Nd:YAG laser. By performing measurements on solutions at different concentrations under various incident laser excitation energies, the nonlinear absorption coefficient, β, and the nonlinear refractive parameter, γ', have been determined (Table S2; for more details on the dependence between β, γ' and the third-order nonlinear susceptibility, $\chi^{(3)}$, see section S12, SI). Most of the O-doped PAHs exhibit negligible NLO absorption and significant NLO refraction. Specifically, only molecules **8**^{Pp} and **5**^{Pp}, displaying significant NLO absorption, show reverse saturable absorption (RSA, β>0) and saturable (SA, β<0) absorption behaviors, respectively (Figure 13). As RSA materials show lower transmission upon increasing the incident laser intensity (*i.e.*, the sample becoming less transparent) and SA materials become progressively more transparent at higher incident laser intensities, both types of NLO absorption behaviors are of great interest for a variety of photonic and opto-electronic applications (*e.g.*, optical limiters, saturable absorbers, etc.). Concerning the NLO refraction, most of toluene solutions of the O-annulated PAHs exhibited self-defocusing (*i.e.,* negative sign nonlinear refractive index parameter γ' values, see Table 5) with the exception of pyranyl derivatives **5**^{Pp} and **6**^{Pp}, which displayed a self-focusing behavior (*i.e.*, positive γ' *values*, see Figure S57, SI). In order to better rationalize these findings, the UV-Vis-NIR absorption spectra of toluene solutions containing the relevant O-annulated PAHs were compared to those obtained from calculations (Figures S60 and S61, SI). Thus, from the comparison between the energy of the lower energy electronic transitions of the different O-doped PAHs studied here and the energy of the laser excitation photons, it becomes evident that different degree of resonant enhancement is expected to occur. In particular, going from molecule **8**^{Fur}, to **5**^{Fur} and then to **6**^{Fur}the lower energy electronic transitions shift to longer wavelengths, getting closer to the laser excitation wavelength and resulting in more efficient resonance enhancement as shown in Table S2, SI. Specficially, the lowest energy electronic transition of molecule **8**^{Fur}, occurring at 357 nm, shifts to 477 nm in the case of **5**^{Fur} and to 534 nm in the case of **6**^{Fur}. Similar observations have been evidenced for the pyranyl counterparts as well. These energy shifts of the lower energy electronic transition give rise to significant resonant enhancement of the NLO response, in line with the general rule according to which the closer is the lowest energy electronic transition to the energy of the laser excitation photon (532 nm), the higher is the degree of resonant enhancement of the NLO response. Therefore, considering the lowest-energy transitions centered at 357, 477 and 534 nm for molecules **8**^{Fur}, **5**^{Fur} and **6**^{Fur}, respectively, the excitation of furanyl derivative **6**^{Fur} gives rise to the highest NLO response. Furthermore, as the sign of the NLO refraction depends on the relative position of the excitation wavelength with respect to the molecular absorption band,[91-93] one can obtain NLO refractions with opposite signs. In particular, as for molecule **5**^{Fur} the excitation occurs at a longer wavelength compared to its lowest-energy absorption band, molecules **5**^{Fur} and **5**^{Pp} exhibit opposite NLO refractions. Along this line, molecules **8**^{Fur}, **8**^{Pp} and **4** were also found to exhibit negative NLO refractions as the excitations take place at longer wavelengths than the lowest-energy absorption bands of the relevant colorant.

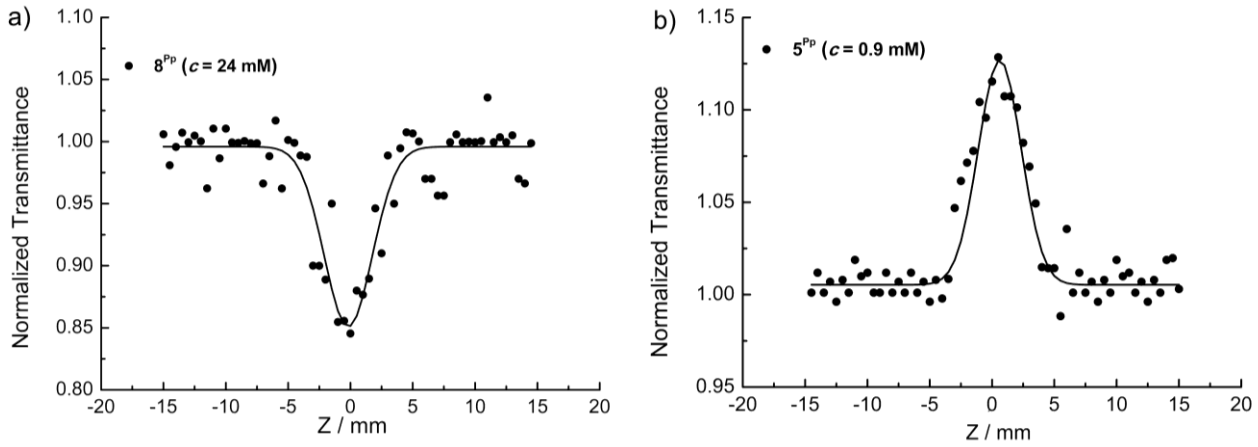

Figure 13. "Open-aperture" Z-scans of solutions containing **8^Pp** (a) and **5^Pp** (b) measured under 35 ps, 532 nm laser excitation.

The third-order susceptibility $\chi^{(3)}$ and the second hyperpolarizability γ have been then deduced (see Tables 5 and S2, SI), identifying a trend within each family of O-annulated compounds. Specifically, starting from model compounds **8^Fur** and **8^Pp**, we can observe an increase of the γ values of two orders of magnitude by extending the molecular π-surface, *i.e.* for molecules **5^Fur/Pp** and **6^Fur/Pp**. To shed further light on this NLO response, we have calculated the electronic static (*i.e.*, when the excitation frequency of the incoming laser beam tends to zero, with $\omega \rightarrow 0$) and the frequency-dependent (i.e., $\omega \neq 0$) second hyperpolarizabilities (Table 6), denoted as $\gamma(0;0,0,0)$ and $\gamma(-\omega;\omega,-\omega,\omega)$ respectively. As one can easily discern from Table 6, $\gamma(0;0,0,0)$ and $\gamma(-\omega;\omega,-\omega,\omega)$ are larger for the pyranopyranyl derivatives compared to those of the furanyl compounds. This is in full agreement with the experimental observations. An exception to this response was found for $\gamma(0;0,0,0)$ of molecules **8^Pp** and **8^Fur**, for which an opposite behaviour was observed, namely $\gamma^{Fur}(0;0,0,0) > \gamma^{Pp}(0;0,0,0)$. As one can observe (see Figure 14a) in the spectral region where the excitation occurs (532 nm), the theoretical $\gamma(-\omega;\omega,-\omega,\omega)$ value for pyranopyranyl derivative **8^Pp** is significantly larger compared to its furanyl analogue **8^Fur**, again in agreement with the experimental findings (see above); furthermore, the large increase of $\gamma(-\omega;\omega,-\omega,\omega)$ value for pyranopyranyl **8^Pp** at about 250 nm, is associated with the significant light absorption of the molecule in the given spectral region. Similar results are evidenced for molecule **5^Pp**, which shows a clear enhancement of the $\gamma_{yyyy}(-\omega;\omega,-\omega,\omega)$ value at *ca.* 500 nm (see Figure 14b). Corroborating the experimental findings, theoretical calculations indicate that $\gamma(0;0,0,0)$ and $\gamma(-\omega;\omega,\omega,\omega)$ are strongly affected by the type of O-annulation, with the pyranyl derivatives displaying the larger values. Finally, the NLO response of the O-doped PAHs studied here was found to be of comparable magnitude with that of some other organic conjugated materials, reported recently and being also promising for photonic and opto-electronic applications.[98,99]

Table 5. Second hyperpolarizability (γ) values of O-doped PAHs dissolved in toluene, determined under 35 ps, 532 nm laser excitation.

Molecule (λ_{max})[a]	$Re\gamma$ ($\times 10^{-31}$ esu)	$Im\gamma$ ($\times 10^{-31}$ esu)	γ ($\times 10^{-31}$ esu)	γ ($\times 10^{-31}$ esu)	$Im\gamma$ ($\times 10^{-31}$ esu)	$Re\gamma$ ($\times 10^{-31}$ esu)	Molecule (λ_{max})[a]
8^Fur (357 nm)	-0.0015±0.0003	-	0.0015±0.0003	0.013±0.002	0.0058±0.002	-0.012±0.002	**8^Pp** (444 nm)
5^Fur (477 nm)	-0.11±0.05	-	0.11±0.05	0.14±0.04	-0.099±0.003	0.094±0.001	**5^Pp** (556 nm)
6^Fur (534 nm)	-0.14±0.05	-	0.14±0.05	1.34±0.20	-	1.34±0.20	**6^Pp** (639 nm)
4 (463 nm)	-0.025±0.005	-	0.025±0.005				

[a] Wavelength of the lowest-energy electronic transition in toluene.

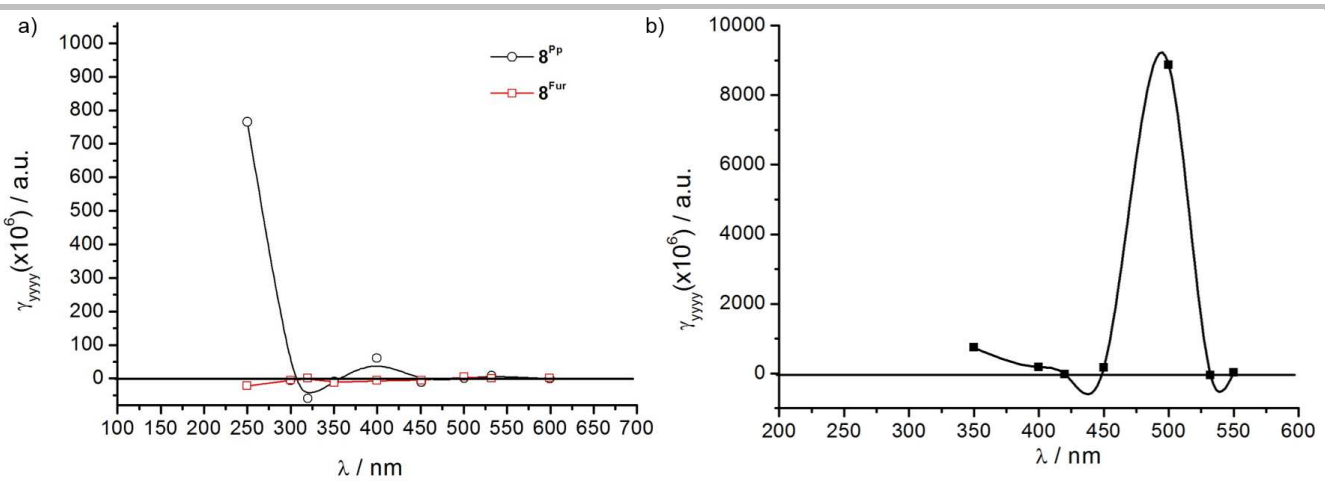

Figure 14. Calculated wavelength dependence $\gamma_{yyyy}(-\omega;\omega,-\omega,\omega)$ profile for **8**^{Pp} and **8**^{Fur} (a) and **5**^{Pp} (b). The values were computed with CAM-B3LYP/6-31+G** method at the gas phase.

In order to study the effect of the dielectric environment (solvent effect) on the NLO response, we have also computed the ρ value, defined as the ratio between the static second-hyperpolarizability values in solution $\gamma(0;0,0,0)^{sol}$ and in the gas phase $\gamma(0;0,0,0)^{gas}$ (Table 6). As one can observe from Figure 15a, the ρ value increases with the extension of the molecular π-surface; also, larger ρ values are found for the planar pyranopyranyl derivatives ($\rho^{Pp} > \rho^{Fur}$). These data suggest that the more extended is the π-surface and the planarity of the molecule, the greater is the effect of the solvent on the NLO response. Moreover, in Figure 15b the dependence between $\gamma(0;0,0,0)$ and E_g^T for derivatives **5**$^{Fur/Pp}$, **6**$^{Fur/Pp}$ and **8**$^{Fur/Pp}$ is depicted. It clearly appears that the decrease of E_g^T leads to an increase of $\gamma(0;0,0,0)$, suggesting that for these molecular scaffolds the tuning of the HOMO and LUMO energy levels greatly affects their NLO response. It is important to emphasize here that the difference of one order of magnitude between the NLO responses of **8**^{Fur} and **8**^{Pp} can be attributed to the change of the degree of molecular planarity, as their lower absorption bands are lying at 357 and 444 nm, respectively, well below the excitation wavelength at 532 nm.

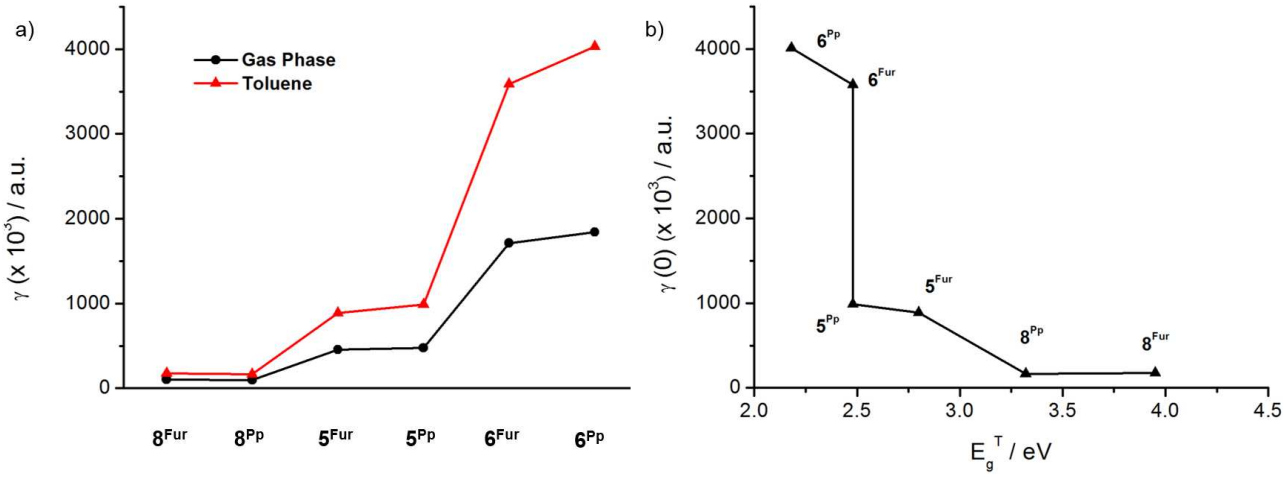

Figure 15. a) The average value of the static second-hyperpolarizability of the studied molecules computed in the gas phase and in toluene solution. b) Variation of the static average second-hyperpolarizability $\gamma(0;0,0,0)$ for the O-annulated PAHs with the E_g^T. The CAM-B3LYP/6-31+G** method was used in the presence of toluene as solvent.

Table 6. The average values of static ($\gamma(0)$) and dynamic second-hyperpolarizabilities ($\gamma(-\omega;\omega,-\omega,\omega)$) of pyranopyranyl and furanyl derivatives. The reported data were calculated at the B3LYP/6-31G**gas phase optimized geometry, by using the CAM-B3LYP/6-31+G** method

Property	**8**^{Fur}	**8**^{Pp}	**5**^{Fur} [b]	**5**^{Pp} [b]	**6**^{Fur} [b]	**6**^{Pp} [b]	**4** [b]
$\rho=\gamma^{sol}/\gamma^{gas}$ [d]	1.68	1.72	1.94	2.07	2.09	2.18	1.74

γ(0;0,0,0) [×10^3] (a.u.)	104 175[d]	96.4 166[d]	457.5 889[d]	476.6 989[d]	1712 3578[e]	1842 4010[e]	627 1094[d]
γ(-ω;ω,-ω,ω) [×10^3] (a.u.)[a]	140 235[e]	2010 3457[e]	-4264 8272[e]	-15770 -32640[e]	-116933 245559[e]	NC[f] -	9110 15860[e]
γ(-ω;ω,-ω,ω) [×10^{-31}] (esu)	0.00145 ±0.00030[g] 0.0012[e,h]	0.0133 ±0.0020[g] 0.017[e,h]	0.113 ±0.050[g] 0.04[e,h]	0.14±0.04[i] -0.16[e,h]	0.138 ±0.050[g] -1.2[e,h]	1.335 ±0.200[g] -	0.025 ±0.005[g] 0.079[e,h]

[a]Frequency-dependent value, λ=532 nm. [b]The *t*Bu groups are substituted with H. [c]γ^{sol}: second hyperpolarizability computed in the presence of the solvent (toluene); γ^{gas}: second hyperpolarizability computed in the gas phase. [d]Value computed in the presence of toluene. [e]Computed by multiplying the gas-phase value with the scaling factor, ρ, presented in the first line, in order to get an estimation of the property in solution. [f]Non-convergence. [g]The experimental value was measured by using the Z-Scan technique, with 35 ps laser excitation at 532 nm (solvent: toluene). [h]The computed value was converted to esu by using the conversion factor 1 a.u.=5.0367 x 10^{-40} esu.

NLO responses in thin films: towards devices. Driven from the promising NLO results obtained in solution, thin films of PMMA containing the relevant dye were prepared by spin coating (thickness of 350-550 nm as measured by a Dektak XT™ stylus profilometer). The results are gathered in Table 7 (details in section S12, SI).[94-95] As thin films present a different dielectric environment compared to that of a liquid solution, different behaviors of NLO responses are observed.[96] The Z-scan measurements were performed under 532 nm, 35 ps laser pulses. The UV-Vis-NIR optical absorption spectra of the prepared thin films are shown in Figures S62-63, SI. While the absorption spectra of the thin films containing the furanyl derivatives were found to closely match those taken from toluene solutions, the absorption profiles of the films containing the pyranopyranyl derivatives (with the exception of those containing molecule **8^{Pp}**) exhibited significant broadening of the main absorption bands, suggesting a non-negligible aggregation of the molecules in PMMA. Concerning the general properties of the thin films, it is important to note that the NLO responses of all films are exclusively dominated by NLO refraction (for the range of incident laser intensities used, *i.e.* up to 30-35 GW/cm^2). No evidences of nonlinear absorption have been observed for laser intensities as high as the damage threshold of the films. These results are a very promising for practical applications as they show high damage thresholds, while the absence of absorption reduces significantly the drawbacks of any thermal effects.[97] As for the magnitude of the NLO refraction (*i.e.*, the real part of the third-order susceptibility, $Re\chi^{(3)}$), thin films containing furanyl derivatives **8^{Fur}** and **5^{Fur}** show very similar values to those obtained from the corresponding toluene solutions (*i.e.*, about 10^{-13} esu). On the other hand, pyranyl derivatives **5^{Pp}**, **6^{Pp}** and **8^{Pp}** values are lower, most probably because of aggregation (see broadening of the UV-Vis absorption profile for the pyranyl molecules in PMMA displayed in Figures S62-63). To assess the exploitability and suitability of the thin-films NLO response for engineering optoelectronic devices, two figures of merit are usually considered: *T* and *W*. These parameters are defined as follows:[94,96]

$T=\beta\lambda/\gamma'<1$ and $W=\Delta n/\alpha\lambda>1$

where β is the nonlinear absorption coefficient, λ is the excitation wavelength, γ' is the nonlinear refractive parameter, $\Delta n = \gamma' I$ is the induced index change and α is the linear absorption coefficient (in cm^{-1}). The first parameter ($T < 1$) infers that the NLO absorption must be weak compared to the NLO refraction, while the second ($W > 1$) suggests that the linear absorption must be relatively weak compared to the nonlinearity. In the present case, the *T* value is always < 1, thus fulfilling the necessary requirements of a negligible NLO absorption of the films (*i.e.*, $\beta \approx 0$). High *W* values ranging between ~390 and 10 are estimated for the less π-extended derivatives **8$^{Fur/Pp}$** and most π-extended **6^{Pp}**, respectively, assuming an intermediate incident laser from those employed. These *W* values are very high and thus very encouraging to further exploit thin films containing pyranopyranyl derivatives in waveguiding devices and optical couplers.[94-96]

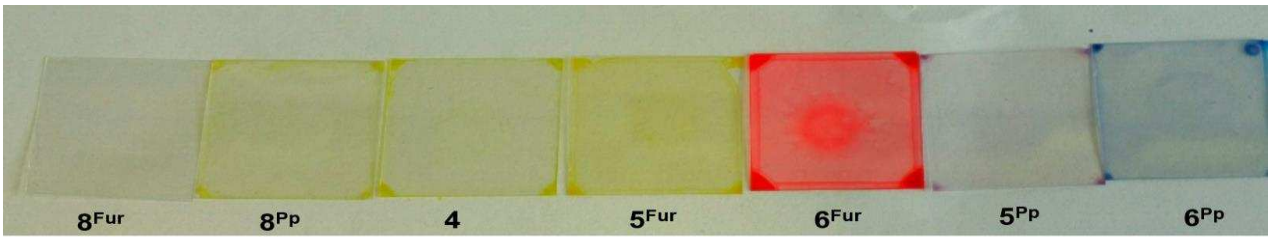

Table 7. Thickness (*L*), nonlinear refractive index parameters (γ' and $Re\chi^{(3)}$) and figure of merit (*W*) of PMMA thin films containing the relevant O-doped PAHs on glass.

Molecule	L (nm)	γ' ($\times10^{-18}$ m^2/W)	$Re\chi^{(3)}$ ($\times10^{-13}$ esu)	W	W	$Re\chi^{(3)}$ ($\times10^{-13}$ esu)	γ' ($\times10^{-18}$ m^2/W)	L (nm)	Molecule
8^{Fur}	367	-0.43±0.02	-0.62±0.03	340	390	-0.37±0.,01	-0.26±0.01	361	**8^{Pp}**
5^{Fur}	377	-1.12±0.02	-1.59±0.03	200	20	-0.94±0.04	-0.66±0.03	391	**5^{Pp}**
6^{Fur}	380	-	-	-	10	-0.70±0.03	-0.49±0.02	383	**6^{Pp}**

Conclusions

In conclusion, in this paper we have described the synthesis of O-doped polyaromatic hydrocarbons, in which two polycyclic aromatic hydrocarbon substructures are fused through furanyl or pyranopyranyl cycles. Starting from the bishydroxyPAHs, acid- and Cu-catalyzed O-annulation reactions allowed the planarization of the molecules through the formation of furanyl or pyranopyranyl rings. Comprehensive photophysical measurements in solution showed that these molecules feature high emission yields (Φ = 0.5 – 0.9) and tunable absorption properties throughout the UV-vis spectral region. Complementary solid-state photophysical studies of the dyes organized in microscopic morphologies showed that only those prepared from the furanyl derivatives retain the emissive molecular properties. Electrochemical investigations showed that in all cases the O-annulation increases the electron donor capabilities by raising the HOMO energy level with the LUMO energy level being less affected. This ultimately causes a shrinking of HOMO-LUMO energy gaps, with the pyranopyranyl planarization triggering the narrower gaps and thus the lowest-energy emissive species. Finally, third-order NLO measurements of solutions containing the relevant dyes displayed significant second hyperpolarizibility, the extent of which depends on the *i*) molecular planarity and *ii*) the HOMO-LUMO energy gap. Theoretical computation of the optoelectronic properties performed with the CAM-B3LYP/6-31+G** method provides reliable data for predicting the excitation spectra, energy gaps and second hyperpolarizability values, for which the pyranopyranyl derivatives display the larger second hyperpolarizability values. In this respect, PMMA films containing the pyranopyranyl derivatives displayed weak linear absorption and NLO absorption compared to the nonlinearity and NLO refraction, respectively, revealing to be prime materials for engineering photonic devices, such as waveguiding and optical couplers or fluorescent probes in lipid bilayer membranes.[100] From these results, it is clear that the potential to build a broad variety of new colorful molecules is apparent. Thus, further investigations will be now centered on the study of different heteroatoms, like the other chalcogens such S, Se and Te atoms, the polarizability of which is expected to further affect the NLO response and finely tune the HOMO-LUMO gap.

Experimental Section

Full experimental details and characterization data, spectroscopic measurments, cyclic voltammograms, computational studies and NLO measurement details are gathered in the Supporting Information. CCDC 1424424-1424428 contain the supplementary crystallographic data for compounds **1c**, **4**, **5^{Fur}**, **6^{Fur}** and **7^{Fur}**. These data can be obtained free of charge from The Cambridge Crystallographic Data Centre via www.ccdc.cam.ac.uk/data_request/cif.

Acknowledgments

D.B. gratefully acknowledges the EU through the ERC Starting Grant “COLORLANDS” project, the Science Policy Office of the Belgian Federal Government (BELSPO-IAP 7/05 project), MIUR through the FIRB Futuro in Ricerca “SUPRACARBON” (contract no. RBFR10DAK6), the "SACS" project (grant number 310651) and the Cardiff University. We thank Ms. Francesca Vita for the SEM analyses, Ms. Maria Mercedes Lorenzo Garcia for the help with ATR analyses, Dr. Caroline A. Ahad Hadad for some TGA measurements and Dr. Domenico Milano for the artwork used in the TOC image. The authors also acknowledge Dr. Simon J. A. Pope for the help with some of the fluorescence lifetime measurements and Panagiotis Aloukos for the precious suggestions and help with the NLO analyses on the thin films.

Keywords: PAHs, O-annulation, heteroatom doping, chromophores, nonlinear optics.

[1] J. Liu, B.-W. Li, Y.-Z. Tan, A. Giannakopoulos, C. Sanchez-Sanchez, D. Beljonne, P. Ruffieux, R. Fasel, X. Feng, K. Müllen, *J. Am. Chem. Soc.* **2015**, *137*, 6097–6103.

[2] X. Li, X. Wang, L. Zhang, S. Lee, H. Dai, *Science* **2008**, *319*, 1229–1232.

[3] L. Chen, Y. Hernandez, X. Feng, K. Müllen, *Angew. Chem. Int. Ed.* **2012**, *51*, 7640–7654.

[4] X. Feng, W. Pisula, K. Müllen, *Pure Appl. Chem.* **2009**, *81*, 2203–2224.

[5] J. E. Anthony, *Angew. Chem. Int. Ed.* **2008**, *47*, 452–483.
[6] J. Wu, W. Pisula, K. Müllen, *Chem. Rev.* **2007**, *107*, 718–47.
[7] M. Cotlet, T. Vosch, S. Habuchi, T. Weil, K. Müllen, J. Hofkens, F. De Schryver, *J. Am. Chem. Soc.* **2005**, *127*, 9760–9768.
[8] U. Lewandowska, W. Zajaczkowski, L. Chen, F. Bouillière, D. Wang, K. Koynov, W. Pisula, K. Müllen, H. Wennemers, *Angew. Chem. Int. Ed.* **2014**, *53*, 12537–12541.
[9] V. Balzani, G. Bergamini, P. Ceroni, E. Marchi, *New J. Chem.* **2011**, *35*, 1944–1954.
[10] L. Rocard, A. Berezin, F. De Leo, D. Bonifazi, *Angew. Chem. Int. Ed.* **2015**, *54*, 15739–15743.
[11] R. S. K. Kishore, O. Kel, N. Banerji, D. Emery, G. Bollot, J. Mareda, A. Gomez-Casado, P. Jonkheijm, J. Huskens, P. Maroni, M. Borkovec, E. Vauthey, N. Sakai, S. Matile, *J. Am. Chem. Soc.* **2009**, *131*, 11106–11116.
[12] A. Wilson, G. Gasparini, S. Matile, *Chem. Soc. Rev.* **2014**, *43*, 1948–1962.
[13] H. Zhylitskaya, J. Cybińska, P. Chmielewski, T. Lis, M. Stępień, *J. Am. Chem. Soc.* **2016**, *138*, 11390-11398.
[14] L. Maggini, D. Bonifazi, *Chem. Soc. Rev.* **2012**, *41*, 211–241.
[15] F. Würthner, *Chem. Commun.* **2004**, 1564–1579.
[16] A. Ajayaghosh, V. K. Praveen, C. Vijayakumar, *Chem. Soc. Rev.* **2008**, *37*, 109–122.
[17] S. S. Babu, J. Aimi, H. Ozawa, N. Shirahata, A. Saeki, S. Seki, A. Ajayaghosh, H. Möhwald, T. Nakanishi, *Angew. Chem. Int. Ed.* **2012**, *51*, 3391–3395.
[18] S. S. Babu, *Phys. Chem. Chem. Phys.* **2015**, *17*, 3950–3953.
[19] S. S. Babu, V. K. Praveen, A. Ajayaghosh, *Chem. Rev.* **2014**, *114*, 1973–2129.
[20] R. Bhosale, J. Míšek, N. Sakai, S. Matile, *Chem. Soc. Rev.* **2010**, *39*, 138–149.
[21] J. Roncali, *Chem. Rev.* **1997**, *97*, 173–206.
[22] J. Roncali, *Macromol. Rapid Commun.* **2007**, *28*, 1761–1775.
[23] X. Wang, G. Sun, P. Routh, D.-H. Kim, W. Huang, P. Chen, *Chem. Soc. Rev.* **2014**, *43*, 7067–7098.
[24] U. N. Maiti, W. J. Lee, J. M. Lee, Y. Oh, J. Y. Kim, J. E. Kim, J. Shim, T. H. Han, S. O. Kim, *Adv. Mater.* **2014**, *26*, 40–67.
[25] W. Jiang, Y. Li, Z. Wang, *Chem. Soc. Rev.* **2013**, *42*, 6113–6127.
[26] A. Mateo-Alonso, *Chem. Soc. Rev.* **2014**, *43*, 6311–6324.
[27] X.-Y. Wang, J.-Y. Wang, J. Pei, *Chem. A Eur. J.* **2015**, *21*, 3528–3539.
[28] M. J. D. Bosdet, W. E. Piers, *Can. J. Chem.* **2009**, *87*, 8–29.
[29] P. G. Campbell, A. J. V. Marwitz, S.-Y. Liu, *Angew. Chem. Int. Ed.* **2012**, *51*, 6074–6092.
[30] D. Bonifazi, F. Fasano, M. M. Lorenzo-Garcia, D. Marinelli, H. Oubaha, J. Tasseroul, *Chem. Commun.* **2015**, *51*, 15222–15236.
[31] X.-Y. Wang, J.-Y. Wang, J. Pei, *Chem. Eur. J.* **2015**, *21*, 3528–3539.
[32] Y. Matano, H. Imahori, *Org. Biomol. Chem.* **2009**, *7*, 1258–1271.
[33] T. Baumgartner, R. Réau, *Chem. Rev.* **2006**, *106*, 4681–4727.
[34] T. Baumgartner, *Acc. Chem. Res.* **2014**, *47*, 1613–1622.
[35] Z. Liu, T. B. Marder, *Angew. Chem. Int. Ed.* **2008**, *47*, 242–244.
[36] M. Stępień, E. Gońka, M. Żyła, N. Sprutta, *Chem. Rev.* **2016**, DOI:10.1021/acs.chemrev.6b00076.
[37] A. Narita, X.-Y. Wang, X. Feng, K. Müllen, *Chem. Soc. Rev.* **2015**, *44*, 6616–6643.
[38] R. Pummerer, E. Prell, A. Rieche, *Chem. Ber.* **1926**, *59*, 2159–2161.
[39] R. Pummerer, A. Rieche, *Chem. Ber.* **1926**, *59*, 2161–2175.
[40] H. Li, F. Zhang, S. Qiu, N. Lv, Z. Zhao, Q. Li, Z. Cui, *Chem. Commun.* **2013**, *49*, 10492–10494.
[41] N. Lv, M. Xie, W. Gu, H. Ruan, S. Qiu, C. Zhou, Z. Cui, *Org. Lett.* **2013**, *15*, 2382–2385.
[42] "Semiconductor Device, Method of Manufacturing the Same, and Method of Forming Multilayer Semiconductor Thin Film": N. Kobayashi, M. Sasaki, T. Ohe, U.S. Patent 8,399,288 B2, **2013**.
[43] "Novel Materials for Organic Electroluminescent Devices": P. Stoessel, A. Buesing, H. Heil, U.S. Patent 2010/0013381 A1, **2010**.
[44] N. Kobayashi, M. Sasaki, K. Nomoto, *Chem. Mater.* **2009**, *21*, 552–556.
[45] D. Stassen, N. Demitri, D. Bonifazi, *Angew. Chem. Int. Ed.* **2016**, *55*, 5947–5951.
[46] M. Hovorka, R. Ščigel, J. Gunterová, M. Tichý, J. Závada, *Tetrahedron* **1992**, *48*, 9503–9516.
[47] M. Hovorka, J. Závada, *Tetrahedron* **1992**, *48*, 9517–9530.
[48] B. Feringa, H. Wynberg, *Bioorg. Chem.* **1978**, *7*, 397–408.
[49] J. Brussee, J. L. G. Groenendijk, J. M. te Koppele, A. C. A. Jansen, *Tetrahedron* **1985**, *41*, 3313–3319.
[50] M. Smrcina, J. Polakova, S. Vyskocil, P. Kocovsky, *J. Org. Chem.* **1993**, *58*, 4534–4538.
[51] M. Noji, M. Nakajima, K. Koga, *Tetrahedron Lett.* **1994**, *35*, 7983–7984.
[52] T. Furuta, K. Tanaka, K. Tsubaki, K. Fuji, *Tetrahedron* **2004**, *60*, 4431–4441.
[53] K. Tsubaki, H. Tanaka, K. Takaishi, M. Miura, H. Morikawa, T. Furuta, K. Tanaka, K. Fuji, T. Sasamori, N. Tokitoh, T. Kawabata, *J. Org. Chem.* **2006**, *71*, 6579–6587.
[54] H. Egami, K. Matsumoto, T. Oguma, T. Kunisu, T. Katsuki, *J. Am. Chem. Soc.* **2010**, *132*, 13633–13635.
[55] K. Tanaka, T. Furuta, K. Fuji, Y. Miwa, T. Taga, *Tetrahedron: Asymmetry* **1996**, *7*, 2199–2202.
[56] S. Wang, B. Lv, Q. Cui, X. Ma, X. Ba, J. Xiao, *Chem. Eur. J.* **2015**, *21*, 14791–14796.
[57] "Blue light emitting material": J. Pillow, S. Kobayashi, M. Humphries, WO2010/013006 A2, **2010**.
[58] C. Zimmermann, F. Willig, S. Ramakrishna, B. Burfeindt, B. Pettinger, R. Eichberger, W. Storck, *J. Phys. Chem. B* **2001**, *105*, 9245–9253.
[59] R. O. Al-Kaysi, T. Sang Ahn, A. M. Müller, C. J. Bardeen, *Phys. Chem. Chem. Phys.* **2006**, *8*, 3453–3459.
[60] L. B. A. Johansson, Y. G. Molotkovsky, L. D. Bergelson, *J. Am. Chem. Soc.* **1987**, *109*, 7374–7381.
[61] D. N. Coventry, A. S. Batsanov, A. E. Goeta, J. A. K. Howard, T. B. Marder, R. N. Perutz, *Chem. Commun.* **2005**, 2172–2174.
[62] A. G. Crawford, Z. Liu, I. A. I. Mkhalid, M.-H. Thibault, N. Schwarz, G. Alcaraz, A. Steffen, J. C. Collings, A. S. Batsanov, J. A. K. Howard, T. B. Marder, *Chem. Eur. J.* **2012**, *18*, 5022–5035.
[63] S. E. Allen, R. R. Walvoord, R. Padilla-Salinas, M. C. Kozlowski, *Chem. Rev.* **2013**, *113*, 6234–6458.
[64] J. Aydin, K. S. Kumar, M. J. Sayah, O. A. Wallner, K. J. Szabó, *J. Org. Chem.* **2007**, *72*, 4689–4697.
[65] M. Nakajima, I. Miyoshi, K. Kanayama, S. Hashimoto, M. Noji, K. Koga, *J. Org. Chem.* **1999**, *64*, 2264–2271.
[66] J. Areephong, N. Ruangsupapichart, T. Thongpanchang, *Tetrahedron Lett.* **2004**, *45*, 3067–3070.
[67] K. Nakanishi, D. Fukatsu, K. Takaishi, T. Tsuji, K. Uenaka, K. Kuramochi, T. Kawabata, K. Tsubaki, *J. Am. Chem. Soc.* **2014**, *136*, 7101–7109.
[68] T. Weil, T. Vosch, J. Hofkens, K. Peneva, K. Müllen, *Angew. Chem. Int. Ed.* **2010**, *49*, 9068–9093.
[69] L. Chen, C. Li, K. Müllen, *J. Mater. Chem. C* **2014**, *2*, 1938–1956.

[70] Z. Yuan, S.-L. Lee, L. Chen, C. Li, K. S. Mali, S. De Feyter, K. Müllen, *Chem. Eur. J.* **2013**, *19*, 11842–11846.
[71] N. G. Pschirer, C. Kohl, F. Nolde, J. Qu, K. Müllen, *Angew. Chem. Int. Ed.* **2006**, *45*, 1401–1404.
[72] A. Bohnen, K.-H. Koch, W. Lüttke, K. Müllen, *Angew. Chem. Int. Ed.* **1990**, *29*, 525–527.
[73] S. Karabunarliev, L. Gherghel, K. H. Koch, M. Baumgarten, *Chem. Phys.* **1994**, *189*, 53.
[74] L. Đorđević, T. Marangoni, T. Miletić, J. Rubio-Magnieto, J. Mohanraj, H. Amenitsch, D. Pasini, N. Liaros, S. Couris, N. Armaroli, M. Surin, D. Bonifazi, *J. Am. Chem. Soc.* **2015**, *137*, 8150–8160.
[75] F. Würthner, A. Sautter, C. Thalacker, *Angew. Chem. Int. Ed.* **2000**, *39*, 1243–1245.
[76] F. Würthner, T. E. Kaiser, C. R. Saha-Möller, *Angew. Chem. Int. Ed.* **2011**, *50*, 3376–3410.
[77] N. Sakai, J. Mareda, E. Vauthey, S. Matile, *Chem. Commun.* **2010**, *46*, 4225–4237.
[78] S.-L. Suraru, F. Würthner, *Angew. Chem. Int. Ed.* **2014**, *53*, 7428–7448.
[79] F. N. Miros, S. Matile, *ChemistryOpen* **2016**, *5*, 219–226.
[80] A. Bolag, J. López-Andarias, S. Lascano, S. Soleimanpour, C. Atienza, N. Sakai, N. Martín, S. Matile, *Angew. Chem. Int. Ed.* **2014**, *53*, 4890–4895.
[81] D.-H. Hwang, S.-K. Kim, M.-J. Park, J.-H. Lee, B.-W. Koo, I.-N. Kang, S.-H. Kim, Z. Taehyoung, *Chem. Mater.* **2004**, *16*, 1298–1303.
[82] M. Iyoda, H. Shimizu, *Chem. Soc. Rev.* **2015**, *44*, 6411–6424.
[83] M. J. Frisch, G. W. Trucks, H. B. Schlegel, G. E. Scuseria, M. A. Robb, J. R. Cheeseman, G. Scalmani, V. Barone, B. Mennucci, G. A. Petersson, H. Nakatsuji, M. Caricato, X. Li, H. P. Hratchian, A. F. Izmaylov, J. Bloino, G. Zheng, J. L. Sonnenberg, M. Hada, M. Ehara, K. Toyota, R. Fukuda, J. Hasegawa, M. Ishida, T. Nakajima, Y. Honda, O. Kitao, H. Nakai, T. Vreven, J. A. Montgomery Jr., J. E. Peralta, F. Ogliaro, M. Bearpark, J. J. Heyd, E. Brothers, K. N. Kudin, V. N. Staroverov, R. Kobayashi, J. Normand, K. Raghavachari, A. Rendell, J. C. Burant, S. S. Iyengar, J. Tomasi, M. Cossi, N. Rega, J. M. Millam, M. Klene, J. E. Knox, J. B. Cross, V. Bakken, C. Adamo, J. Jaramillo, R. Gomperts, R. E. Stratmann, O. Yazyev, A. J. Austin, R. Cammi, C. Pomelli, J. W. Ochterski, R. L. Martin, K. Morokuma, V. G. Zakrzewski, G. A. Voth, P. Salvador, J. J. Dannenberg, S. Dapprich, A. D. Daniels, Ö. Farkas, J. B. Foresman, J. V. Ortiz, J. Cioslowski, D. J. Fox, *Gaussian* 09, Revision *A1*, *Gaussian, Inc., Wallingford CT* **2009**.
[84] A. D. Becke, *Phys. Rev. A* **1988**, *38*, 3098–3100.
[85] C. Lee, W. Yang, R. Parr, *Phys. Rev. B* **1988**, *37*, 785–789.
[86] M. D. Hanwell, D. E. Curtis, D. C. Lonie, T. Vandermeerschd, E. Zurek, G. R. Hutchison, *J. Cheminform.* **2012**, *4*, 17.
[87] R. E. Martin, F. Diederich, *Angew. Chem. Int. Ed.* **1999**, *38*, 1350–1377.
[88] A. J. Berresheim, M. Müller, K. Müllen, *Chem. Rev.* **1999**, *99*, 1747–1786.
[89] T. M. Figueira-Duarte, K. Müllen, *Chem. Rev.* **2011**, *111*, 7260–7314.
[90] K. A. Peterson, D. Figgen, E. Goll, H. Stoll, M. Dolg, *J. Chem. Phys.* **2003**, *119*, 11113–11123.
[91] R. W. Boyd, *Nonlinear Optics*, Academic Press, San Diego, CA, **1992**, p. 176.
[92] E. Xenogiannopoulou, M. Medved, K. Iliopoulos, S. Couris, M. G. Papadopoulos, D. Bonifazi, C. Sooambar, A. Mateo-Alonso, M. Prato, *ChemPhysChem* **2007**, *8*, 1056–1064.
[93] L. Đorđević, T. Marangoni, F. De Leo, I. Papagiannouli, P. Aloukos, S. Couris, E. Pavoni, F. Monti, N. Armaroli, M. Prato, D. Bonifazi, *Phys. Chem. Chem. Phys.* **2016**, *18*, 11858–11868.
[94] L. Brzozowski, E. H. Sargent, *J. Mater. Sci. Mater. Electron.* **2001**, *12*, 483–489.
[95] P. W. Smith, *Bell Syst. Tech. J.* **1982**, *61*, 1975–1993.
[96] G. I. Stegeman in *Nonlinear Optical Properties of Advanced Materials, Proc. SPIE, Vol. 1852.*, **1993**, p. 75.
[97] J. L. Bredas, C. Adant, P. Tackx, A. Persoons, B. M. Pierce, *Chem. Rev.* **1994**, *94*, 243–278.
[98] I. Fuks-Janczarek, J-M. Nunzi, B. Sahraoui, I.V. Kityk, J. Berdowski, A.M. Caminade, J.-P. Majoral, A.C. Martineau, P. Frere, J. Roncali, *Optics Communications* **2002**, *209*, 461-466.
[99] B. Sahraoui, J. Luc, A. Meghea, R. Czaplicki, J.L. Fillaut, A. Migalska-Zalas, *J. Opt. A: Pure App. Opt.* **2009**, *11*, 024005.
[100] T. Takeuchi, S. Matile, *Chem. Commun.* **2013**, *49*, 19-29.